STUDIES ON SULFUR DIOXIDE GAS SENSORS USING SODIUM SULFATE-BASED SOLID ELECTROLYTES

1986

NOBUHITO IMANAKA

STUDIES ON SULFUR DIOXIDE GAS SENSORS USING SODIUM SULFATE-BASED SOLID ELECTROLYTES

(硫酸ナトリウム固体電解質を母体とした
亜硫酸ガスセンサに関する研究)

1986

NOBUHITO IMANAKA

PREFACE

The work described in this thesis was carried out under the guidance from Professor Jiro Shiokawa at the Department of Applied Chemistry, Faculty of Engineering, Osaka University.

The object of this thesis is to prepare the appropriate materials for a sulfur dioxide gas sensor using sodium sulfate-based solid electrolytes and examine their practical applications. The author hopes that the work described in this thesis would contribute to the development of a new sulfur dioxide gas sensor.

Nobuhito Imanaka

Suita, Osaka
January, 1986

CONTENTS

Chapter 1

GENERAL INTRODUCTION

As is well-known, sulfur oxides and nitrogen oxides exhausted into air, which can result in acid rain, have caused serious deterioration of the environment. The potential need for regulation of SO_x and NO_x gases in combustion emissions is, nowadays, becoming an important research area.

For practical measurements, several techniques for SO_2 analysis have been widely adopted as follows:

(a) The electrical conductivity measurement of an absorbed solution

(b) Infrared absorption analysis

(c) Ultra-violet spectrum photometric analysis

(d) Flame photometry

(e) Stationary potential electrolysis

(f) Lead dioxide method(An elementary SO_2 gas measurement)

However, the apparatus for these methods((a)-(e)) is expensive and complicated. Recently, a concentration cell method using a solid electrolyte[1, 2] has become of interest for an SO_2 gas detection. A potential advantage of this technique is that monitering for SO_2 can be undertaken simply, selectively, and continuously with low cost.

As the electrolytes, alkali metal sulfates (M=Li, Na, K)[3-11], β-Alumina[12-15], and NASICON[16, 17] have been

examined. Alkali metal sulfates are cation conductors at elevated temperature(>700^{o}C). β-Alumina is one of the other representative cation conductors. NASICON is one of the most widely used materials[18-25] that have been utilized as cation conductors. Both of them are superior in waterproof and abrasion-durability. However, they are not commercially available at present. In addition, β-Alumina and NASICON materials are considerably more expensive than alkali metal sulfates. The electrical conductivity of potassium sulfate is appreciably low compared with sodium sulfate because the cationic radius of K^{+} is larger than that of Na^{+}. Lithium sulfate is not good candidate for the solid electrolyte because of its hygroscopic property and the large endothermal reaction in the course of a phase transition. Sodium sulfate also has several disadvantages. One is the phase transformation[26-42]. By this transformation, cracks occur in the electrolyte body and result in the permeation of ambient gases. Another disadvantage is its low electrical conductivity. Mono, di, or tri-valent cations[43-47] have been doped so as to enhance its conductivity. Furthermore, it is difficult to obtain SO_2-SO_3 equilibrium on the surface of the electrolyte.

General introduction was presented in chapter 1.

In chapter 2, sodium vanadate and rare earth sulfates were doped in order to promote the oxidation from SO_2 to SO_3 and enhance the electrical conductivity, respectively. The suppression of the phase transition was also attempted by these doping. The electromotive force

(EMF) was measured with the appropriate samples for the solid electrolyte by constructing the SO_2 gas concentration cell.

In chapter 3 and 4, for the purpose of developing the solid electroyte which can be utilized at 973 K, rare earth sulfate, and silicon dioxide or aluminum oxide were mixed so as to increase the conductivity and prevent the electrolyte from becoming ductile, respectively. The effort to suppress the phase transition was also made by these mixing. Platinum sputtering on the center surface of the electrolyte was attempted in order to improve the EMF characteristics in the lower SO_2 gas concentration.

In chapter 5, lithium sulfate was mixed as the fourth composition in the Na_2SO_4-$Ln_2(SO_4)_3$-SiO_2 electrolyte so as to make Na^+ cation migrate easier at temperatures lower than 700^oC.

In chapter 6, the solid reference electrode method (metal sulfate-metal oxide electrode) was investigated with the appropriate Na_2SO_4-$Y_2(SO_4)_3$-SiO_2 electrolyte in order to make the apparatus more compact, lighter, and less expensive. Furthermore, the solid reference electrode method with both Na_2SO_4-$Ln_2(SO_4)_3$-Al_2O_3 and Na_2SO_4-Li_2SO_4-$Y_2(SO_4)_3$-SiO_2 solid electrolytes was examined.

In chapter 7, concluding remarks were presented.

The contents of this thesis are composed of the following papers.

(1) Electrical and Thermal Properties of Na_2SO_4 Doped with $NaVO_3$, $Ln_2(SO_4)_3$(Ln=Eu,Pr)

N. Imanaka, G. Adachi, and J. Shiokawa

Can. J. Chem., 61, 1557 (1983).

(2) Properties of sodium sulfate doped with sodium vanadate and $Ln_2(SO_4)_3$(Ln=Eu, Pr) as a solid electrolyte for a sulfur dioxide detector

N. Imanaka, G. Adachi, and J. Shiokawa

Denki Kagaku oyobi Kogyo Butsuri Kagaku, 51, (1), 93 (1983).

(3) Properties of Na_2SO_4 Doped with $NaVO_3$ and $Pr_2(SO_4)_3$ as a Solid Electrolyte

N. Imanaka, G. Adachi, and J. Shiokawa

Chem. Lett., (1983) 287.

(4) Na_2SO_4 Doped with $NaVO_3$ and/or $Ln_2(SO_4)_3$(Ln=Rare Earths) as an SO_2 Solid Electrolyte Sensor

N. Imanaka, G. Adachi, and J. Shiokawa

Proc. the International Meeting on Chemical Sensors, Fukuoka 1983, ed. by T. Seiyama et al.(Kodansha and Elsevier) p. 348.

(5) Sodium Sulfate Doped with Sodium Vanadate and Rare Earth Sulfate as a Solid Electrolyte for a Sulfur Dioxide Gas Detector

N. Imanaka, G. Adachi, and J. Shiokawa

Bull. Chem. Soc. Jpn., 57, 687 (1984).

(6) Sodium Sulfate Mixed with Rare Earth Sulfates(Ln=Y and Gd) and Silicon Dioxide as a Solid Electrolyte for a Sulfur Dioxide Detector

N. Imanaka, Y. Yamaguchi, G. Adachi, and J. Shiokawa

Bull. Chem. Soc. Jpn., 58, 5 (1985).

(7) Sulfur Dioxide Gas Detection with Na_2SO_4-$Y_2(SO_4)_3$-SiO_2 Solid Electrolyte by a Solid Reference Electrode Method

N. Imanaka, Y. Yamaguchi, G. Adachi, and J. Shiokawa

J. Electrochem. Soc., 132, 2519 (1985).

(8) Sodium Sulfate Mixed with Rare Earth Sulfates and Silicon Dioxide as a Solid Electrolyte for a Sulfur Dioxide Detector

N. Imanaka, G. Adachi, and J. Shiokawa

ACS Symposium on Chemical Sensors-Fundamental and Applications, in press.

(9) The Electrical and Thermal Properties of Sodium Sulfate Mixed with Lanthanum Sulfate and Aluminum Oxide

N. Imanaka, Y. Yamaguchi, G. Adachi, J. Shiokawa, and H. Yoshioka

Solid State Ionics, in press.

(10) The Electrical and Thermal Properties of Sodium Sulfate Mixed with Lithium Sulfate, Yttrium Sulfate, and Silicon Dioxide

N. Imanaka, Y. Yamaguchi, G. Adachi, and J. Shiokawa

J. Electrochem. Soc., in contribution.

Chapter 2

THE ELECTRICAL AND THERMAL PROPERTIES OF SODIUM SULFATE DOPED WITH SODIUM VANADATE AND RARE EARTH SULFATES(Ln=Eu, Pr, Y)

2-1. Introduction

Attempts have been made to utilize sodium sulfate as a solid electrolyte for a sulfur dioxide gas sensor. However, in practical use, a phase transformation from Na_2SO_4-I(a high temperature phase) to Na_2SO_4-III(a low temperature phase) is a serious obstacle. In addition, other disadvantages in using sodium sulfate alone as an electrolyte are its lower electrical conductivity and difficulty in obtaining an SO_2-SO_3 equilibrium on the surface of the electrolyte.

In this chapter, efforts of doping with rare earth sulfates and sodium vanadate into sodium sulfate on the electrical conducitvity and on the phase transformation of the solid solutions are examined, and also EMF measurements by applying Na_2SO_4-$NaVO_3$-$Ln_2(SO_4)_3$(Ln=Pr and Y) as an electrolyte for an SO_2 gas concentration cell are to be discussed.

2-2. Experimental

Materials. Rare earth sulfate was prepared by adding a

concentrated H_2SO_4 into rare earth oxide. Sodium vanadate was synthesized by heating the mixture of Na_2CO_3 and NH_4VO_3 (by molar ratio 1:2) at 823 K for 5 h in air. Sodium sulfate, which is hygroscopic, and sodium vanadate were preheated before weighing. Rare earth sulfates were also heated to eliminate the included water. Since they easily absorb water, the real concentration of lanthanoid cation in the mixture was determined by the EDTA titration. Preheated materials were cooled in a desiccator, weighed, and mixed thoroughly in an agate mortar. A mixture of appropriate amount of Na_2SO_4 and $Ln_2(SO_4)_3$(Ln Eu, Pr, and Y) were pelletized and heated at 1073 K for 3 h in air. In Na_2SO_4-$NaVO_3$-$Ln_2(SO_4)_3$ (Ln=Eu, Pr, and Y) systems, the heated pellets were ground, remade into pellets and sintered 3 h at 1073 K in air.

Measurements. Phases and thermal properties were measured with X-ray diffraction method and thermal analysis from Rigaku's Rotaflex and Rigaku's Thermoflex, respectively. Electrical conductivity measurements were carried out by a complex impedance method[48] using a Hewlett Packard vector impedance meter 4800A. The apparatus for the electrical conductivity measurements is shown in Fig. 1. EMF measurements were performed by constructing an SO_2 gas concentration cell which is depicted in Fig. 2. The inner quartz tube compartment was separated by spring loading the electrolyte with a quartz rod. A gold O-ring was used in order to separate the test and the reference SO_2 gas completely. The SO_2 gas concentration was regulated by changing SO_2 and O_2 gas flow rate. A Pt net was applied as an electrode so that the electrolyte could maintain good contact with the SO_2 gas. EMF

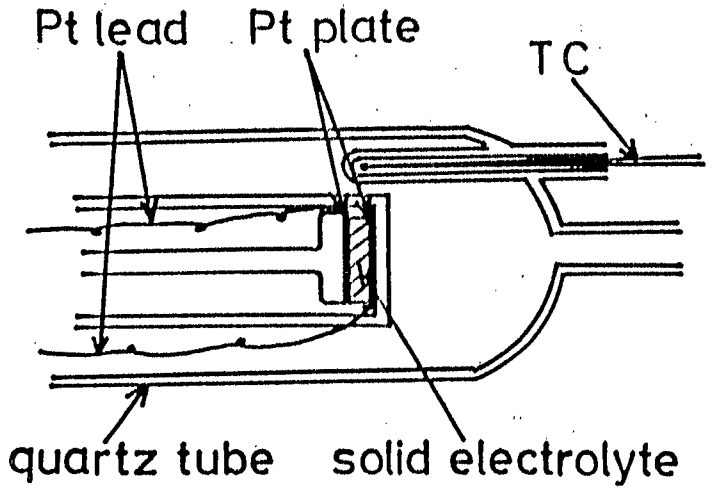

Fig. 1. The apparatus for the electrical conductivity measurements.

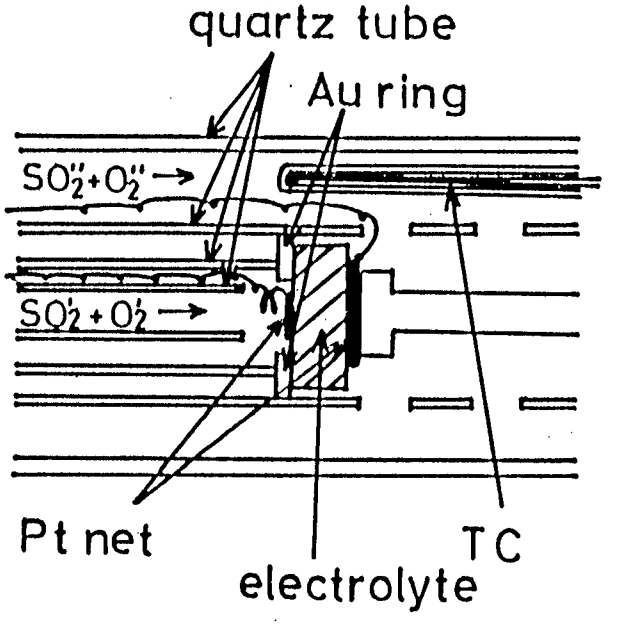

Fig. 2. The apparatus for the electromotive force(EMF) measurements.

measurements were performed with a Takeda Riken Digital Multimeter TR-6855. The response time, which is here defined as the time required from the test gas arrival at the electrolyte in the attainment of about 96% of the calculated EMF, was also measured.

Electromotive force(EMF) calculation. The following equation (I) for test SO_2 and O_2 mixed gas was obtained from the equation(10) in the paper of Jacob and Rao[3].

$$K_4\alpha(1+\eta_{O_2}+\eta_{Ar}-\alpha/2)^{1/2} = (1-\alpha)(\eta_{O_2}-\alpha/2)^{1/2} \quad \text{(I)}$$

In our experiment, sulfur dioxide gas was mixed only with oxygen gas. Therefore, η_{Ar} is equal to zero. Then, the equation(I) is transformed to (II).

$$K_4\alpha(1+\eta_{O_2}-\alpha/2)^{1/2} = (1-\alpha)(\eta_{O_2}-\alpha/2)^{1/2} \quad \text{(II)}$$

This cubic equation of α for (II) is solved by the Newton's method. From the knowledge of K_4, η_{O_2}, and α, the equilibrium partial pressures for SO_3 and O_2 are determined from the next equations.

$$p_{SO_3} = \alpha/(1+\eta_{O_2}-\alpha/2) \quad \text{(III)}$$

$$p_{O_2} = (\eta_{O_2}-\alpha/2)/(1+\eta_{O_2}-\alpha/2) \quad \text{(IV)}$$

(The equations (III) and (IV) are derived from the equations (7) and (8) in Jacob and Rao's paper, respectively.)

In the same way, the reference p_{SO_3}' and p_{O_2}' are calculated. Then, the electromotive force(EMF) was obtained by a following equation(V).

$$E = \frac{RT}{2F} \ln \frac{p_{SO_3}\, p_{O_2}^{1/2}}{p_{SO_3}'\, p_{O_2}'^{1/2}} \quad \text{(V)}$$

Where, R, F, and T are gas constant, Faraday constant, and absolute temperature, respectively. (The equation (V) is

given by the equation(17) in Jacob and Rao's paper.)

2-3. Results and Discussion

Electrical conductivity, phase, and thermal properties.

Two component systems

Na_2SO_4-$Eu_2(SO_4)_3$ system

The phases and thermal results of Na_2SO_4-$Eu_2(SO_4)_3$ are listed in Table 1. Sodium sulfate doped with 0.7 mol% exhibits phase α which is similar to the Na_2SO_4-III phase including a starting material(Na_2SO_4-V phase). The other two samples show phase γ which is different from any Na_2SO_4 phase. All samples exhibit an endothermal peak in DTA curves, indicating that the phase transformation still exists. The electrical conductivity results for Na_2SO_4-$Eu_2(SO_4)_3$ is presented in Fig. 3. Na_2SO_4 and Na_2SO_4 doped with 0.9 mol% $Eu_2(SO_4)_3$ exhibited a discontinuity due to the phase

Table 1. The phases and thermal properties of Na_2SO_4-$Eu_2(SO_4)_3$

Na_2SO_4 (mol%)	$Eu_2(SO_4)_3$ (mol%)	Phases[a]	DTA peaks[b] (K)
99.3	0.7	α + Na_2SO_4-V	493
95.9	4.1	γ + Na_2SO_4-V	553
91.8	8.2	γ + Na_2SO_4-V	563, 573, 818, 1003

[a]The α phase is similar to the Na_2SO_4-III phase (15, 16); the γ phase is different from any Na_2SO_4 phase; Na_2SO_4-V is the initial raw material. X-ray analyses were done at room temperature.

[b]Reproducibility of DTA temperature is within 2 K.

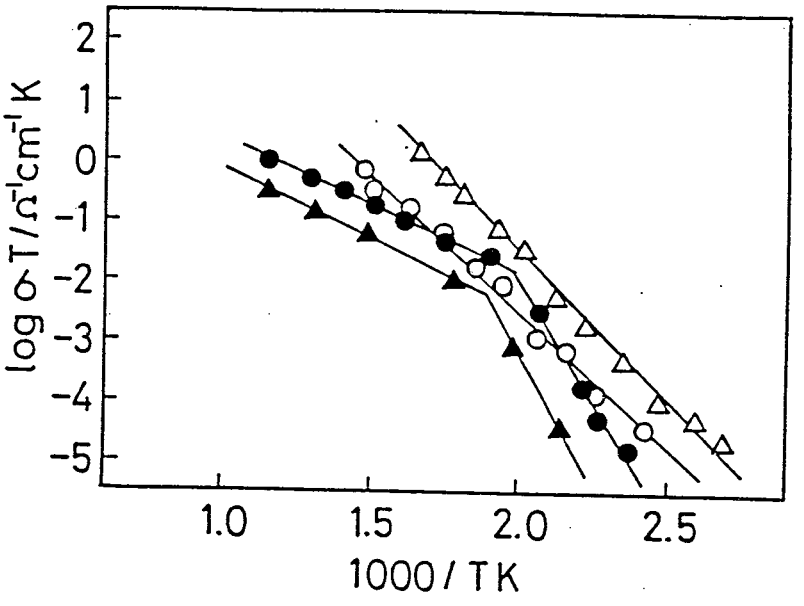

Fig. 3. Temperature dependences of electrical conductivities for Na_2SO_4-$Eu_2(SO_4)_3$

- ● Na_2SO_4:$Eu_2(SO_4)_3$=99.3:0.7
- △ Na_2SO_4:$Eu_2(SO_4)_3$=95.9:4.1
- ○ Na_2SO_4:$Eu_2(SO_4)_3$=91.8:8.2
- ▲ Na_2SO_4

transition from Na_2SO_4-I to Na_2SO_4-III. On the other hand, the samples doped with more than 0.7 mol% $Eu_2(SO_4)_3$ exhibited no change in slope. By doping $Eu_2(SO_4)_3$ into Na_2SO_4, cation vacancies were produced to increase the electrical conductivity and described as $(Na_{(2-3x)/2}Eu_{x/2}\square_x)_2SO_4$, where $\square$ is a cation vacancy. In the case of Na_2SO_4 doped with 4.1 mol% $Eu_2(SO_4)_3$ and 8.2 mol% $Eu_2(SO_4)_3$, $(Na_{0.88}Eu_{0.04}\square_{0.08})_2SO_4$ and $(Na_{0.79}Eu_{0.07}\square_{0.14})_2SO_4$ were formed. In the Na_2SO_4-$Eu_2(SO_4)_3$ system, Na_2SO_4 doped with 4.1 mol% $Eu_2(SO_4)_3$ exhibited the highest electrical conductivity. By doping 8.2 mol% $Eu_2(SO_4)_3$

into Na_2SO_4, its electrical conductivity is about one-tenth that for Na_2SO_4 doped with 4.1 mol% $Eu_2(SO_4)_3$. The reason why Na_2SO_4 doped with 4.1 mol% $Eu_2(SO_4)_3$ exhibited the highest electrical conductivity in the Na_2SO_4-$Eu_2(SO_4)_3$ system may be attributed to the fact that the vacancies produced by doping of Eu^{3+} have a tendency to make clusters when $Eu_2(SO_4)_3$ is dissolved more than 4.1 mol%.

Na_2SO_4-$Pr_2(SO_4)_3$ system

The X-ray and thermal properties of Na_2SO_4-$Pr_2(SO_4)_3$ are listed in Table 2. Sodium sulfate doped with 0.9 mol% or 1.6 mol% $Pr_2(SO_4)_3$ exhibits phase α which is similar to the Na_2SO_4-III phase including a starting material (Na_2SO_4-V phase). The other two samples show phase γ which is different from any Na_2SO_4 phase. All samples exhibit an endothermal peak in DTA curves, indicating that the phase transformation still exists. Electrical conductivity measurements in the system of Na_2SO_4-$Pr_2(SO_4)_3$ are shown in Fig. 4. Doping $Pr_2(SO_4)_3$

Table 2. The phases and thermal properties of Na_2SO_4-$Pr_2(SO_4)_3$.

Sample No.	Na_2SO_4 (mol%)	$Pr_2(SO_4)_3$ (mol%)	Phases	DTA peaks T/K
1	99.1	0.9	α+Na_2SO_4-V	573
2	98.4	1.6	α+Na_2SO_4-V	573
3	95.2	4.8	γ	573
4	90.7	9.3	γ	853

α phase is similar to phase Na_2SO_4-III.[18,19] γ phase is different from any Na_2SO_4 phase.

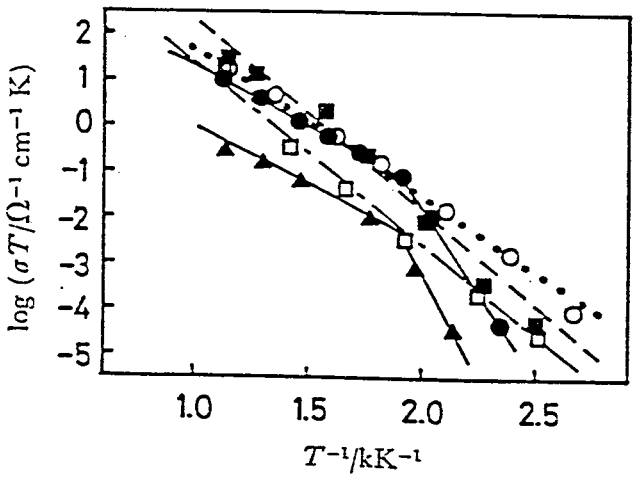

Fig. 4. Temperature dependences of electrical conductivities for Na_2SO_4-$Pr_2(SO_4)_3$.

- ● Na_2SO_4:$Pr_2(SO_4)_3$=99.1:0.9
- ○ Na_2SO_4:$Pr_2(SO_4)_3$=98.4:1.6
- ■ Na_2SO_4:$Pr_2(SO_4)_3$=95.2:4.8
- □ Na_2SO_4:$Pr_2(SO_4)_3$=90.7:9.3
- ▲ Na_2SO_4

into Na_2SO_4 increases the concentration of cation vacancies of the sulfate, and then the electrical conductivity enhances. A break or bend in log(σT) vs. 1/T curves is due to the phase transformation in the sulfate. The solid solution of sodium sulfate doped with 1.6 mol% $Pr_2(SO_4)_3$ did not exhibit any break. The Ⅲ-Ⅰ phase transformation appeared to be fairly suppressed. However, the phase transformation was found to still remain on DTA measurement. The sulfate doped with 4.8 mol% $Pr_2(SO_4)_3$ gives the highest electrical conductivity(from 571 K to 873 K) in the Na_2SO_4-$Pr_2(SO_4)_3$ system.

This fact means that the number of cation vacancies which is effective for cation conduction becomes a maximum with the doping. By doping $Pr_2(SO_4)_3$ more than 4.8 mol%, cation vacancies appear to make clusters and then the electrical conductivity in Na_2SO_4-$Pr_2(SO_4)_3$ system rather decreases.

Na_2SO_4-$Y_2(SO_4)_3$ system

The phases and thermal properties of Na_2SO_4 doped with $Y_2(SO_4)_3$ is listed in Table 3. Sodium sulfate doped with 1.0 mol% $Y_2(SO_4)_3$ shows similar phase to Na_2SO_4-III along with Na_2SO_4-V phase. In the samples of Na_2SO_4 doped with 2.0, 5.0 mol% $Y_2(SO_4)_3$, they exhibit Na_2SO_4-I similar phase. Sodium sulfates doped with $Y_2(SO_4)_3$ more than 7.0 mol% show γ phase which is different from any Na_2SO_4 phase. From thermal

Table 3. The phases and thermal properties of Na_2SO_4-$Y_2(SO_4)_3$.

sample NO.	Na_2SO_4 (mol%)	$Y_2(SO_4)_3$ (mol%)	phases	DTA peaks (K)
1	99.0	1.0	α+Na_2SO_4-V	523
2	98.0	2.0	β	513
3	95.0	5.0	β	613
4	93.0	7.0	γ	603
5	90.0	10.0	γ	793

Phase α is similar to Na_2SO_4-II phase.
Phase β is similar to Na_2SO_4-I phase.
Phase γ is different from any Na_2SO_4 phase.

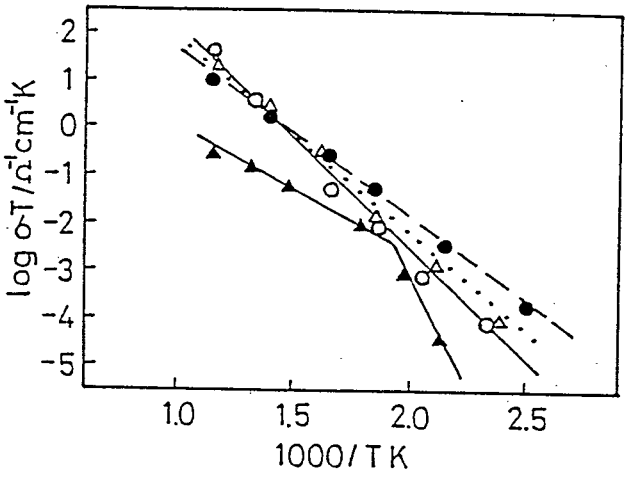

Fig. 5. Temperature dependences of electrical conductivities for Na_2SO_4-$Y_2(SO_4)_3$.

- ● Na_2SO_4:$Y_2(SO_4)_3$=98.0:2.0
- △ Na_2SO_4:$Y_2(SO_4)_3$=95.0:5.0
- ○ Na_2SO_4:$Y_2(SO_4)_3$=90.0:10.0
- ▲ Na_2SO_4

analysis, all Na_2SO_4-$Y_2(SO_4)_3$ samples exhibit phase transition. The electrical conductivity results for Na_2SO_4-$Y_2(SO_4)_3$ are presented in Fig. 5. By doping of 2.0 mol% $Y_2(SO_4)_3$, the conductivity became maximum. Further $Y_2(SO_4)_3$ doping makes the σ value decrease. This is also ascribed to the effect of the cation clustering.

Na_2SO_4-$NaVO_3$ system

In the Na_2SO_4-$NaVO_3$ system, Na_2SO_4 doped with 2 mol% $NaVO_3$, 5 mol % $NaVO_3$, 7 mol% $NaVO_3$, and 10 mol% $NaVO_3$, where these mol% are initial concentrations of the dopant, were prepared. The phases and thermal properties of Na_2SO_4-$NaVO_3$ are summarized in Table 4. From X-ray analysis, Na_2SO_4-$\bar{V}$

Table 4. The phases and thermal properties of Na_2SO_4-$NaVO_3$.

Na_2SO_4 (mol%)	$NaVO_3$ (mol%)	Phases[a]	DTA peaks[b] (K)
98	2	α + Na_2SO_4-V	533, 888
95	5	α + Na_2SO_4-V + trace $NaVO_3$	528, 888
93	7	α + trace Na_2SO_4-V + trace $NaVO_3$	528, 878
90	10	α + trace Na_2SO_4-V + trace $NaVO_3$	523, 873

[a]The α phase is similar to Na_2SO_4-III (15, 16); Na_2SO_4-V and $NaVO_3$ are the initial raw materials. X-ray analyses were done at room temperature.
[b]Reproducibility of DTA temperature is within 5 K.

still remain in all samples and $NaVO_3$ remained in most samples except for Na_2SO_4 doped with 2 mol% $NaVO_3$. These results are probably due to the low solubility of $NaVO_3$ in solid Na_2SO_4. By a DTA measurement, some peaks due to phase transformations are observed in all samples listed in Table 4. Electrical conductivities are greatly lowered by the doping in all samples. A representative behavior is shown in Fig. 6. The structure of Na_2SO_4 is partially destroyed by doping of $NaVO_3$. Doping with $NaVO_3$ does not affect the electrical charge balance. Electrical conductivities of the two-component system Na_2SO_4-$NaVO_3$ are very low. Doping of a third component to the Na_2SO_4-$NaVO_3$ system is necessary in order to improve the electrical conductivities.

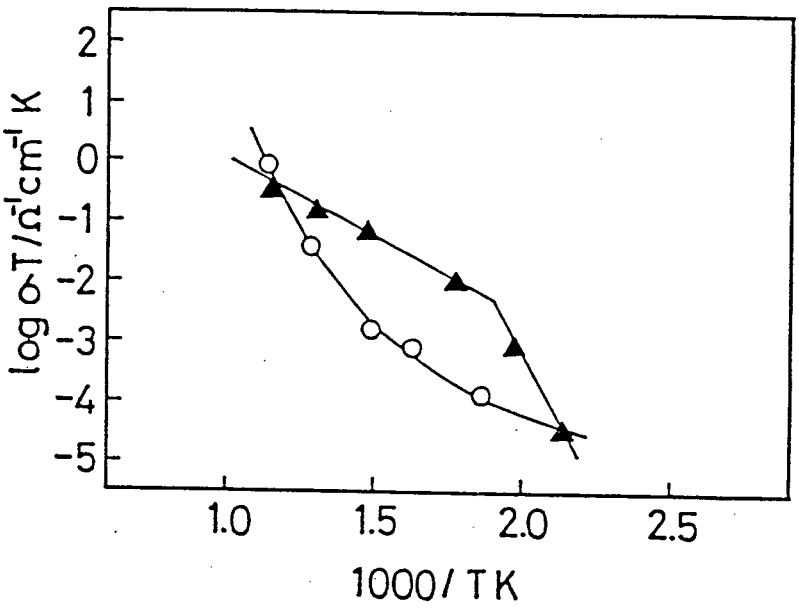

Fig. 6. Temperature dependences of electrical conductivities for Na_2SO_4-$NaVO_3$.

○ Na_2SO_4:$NaVO_3$=95:5

▲ Na_2SO_4

Three-component sysyems

Na_2SO_4-$NaVO_3$-$Eu_2(SO_4)_3$ system

The phases and thermal properties of Na_2SO_4-$NaVO_3$-$Eu_2(SO_4)_3$ are summarized in Table 5. From X-ray analysis, peaks due to the raw materials, $NaVO_3$ and $Eu_2(SO_4)_3$, have disappeared in all samples. The samples that showed α phase are No. 1 and 2. The samples that exhibited β phase are No. 3, 4, and 5. The α and β phases are similar to the Na_2SO_4-III phase(a low temperature phase) and the Na_2SO_4-I(a high temperature phase), respectively. In a DTA measurement, the samples that exhibited the α phase show some endothermal

Table 5. The phases and thermal properties of Na_2SO_4-$NaVO_3$-$Eu_2(SO_4)_3$.

Na_2SO_4 (mol%)	$NaVO_3$ (mol%)	$Eu_2(SO_4)_3$ (mol%)	Phases[a]	DTA peaks[b] (K)
98.1	0.9	1.0	α	493
96.3	1.7	2.0	α	398, 458
94.6	2.4	3.0	β	573 (small)
93.2	2.8	4.0	β	—
91.0	4.0	5.0	β	—

[a] The α and β phases are similar to the Na_2SO_4-III and Na_2SO_4-I phases, respectively (15, 16). X-ray analyses were done at room temperature.
[b] Reproducibility of DTA temperature is within 5 K.

peaks, due to phase transformations. On the other hand, the samples that exhibited the β-phases show no endothermal peak, which means no phase transition occurred. Therefore, the samples that exhibited the β phase in the Na_2SO_4-$NaVO_3$-$Eu_2(SO_4)_3$ system have potential as solid electrolytes for an SO_2 detector concentration cell. Electrical conducitvities of the Na_2SO_4-$NaVO_3$-$Eu_2(SO_4)_3$ samples which exhibit the β phase are shown in Fig. 7. Compared with Na_2SO_4, the electrical conductivities increased about 1.0-2.0 orders of magnitude and the break in the $\log(\sigma T)$ vs. $10^3/T$ relation disappeared. Electrical conductivities enhanced with increasing the concentration of the dopants $NaVO_3$ and $Eu_2(SO_4)_3$, that is, the doping of $NaVO_3$ hardly influences the conductivity of the samples. The samples of Na_2SO_4-$NaVO_3$-$Eu_2(SO_4)_3$ which exhibited the β phase maintain the structure of the Na_2SO_4-I phase even at a relatively low temperature. Therefore, the

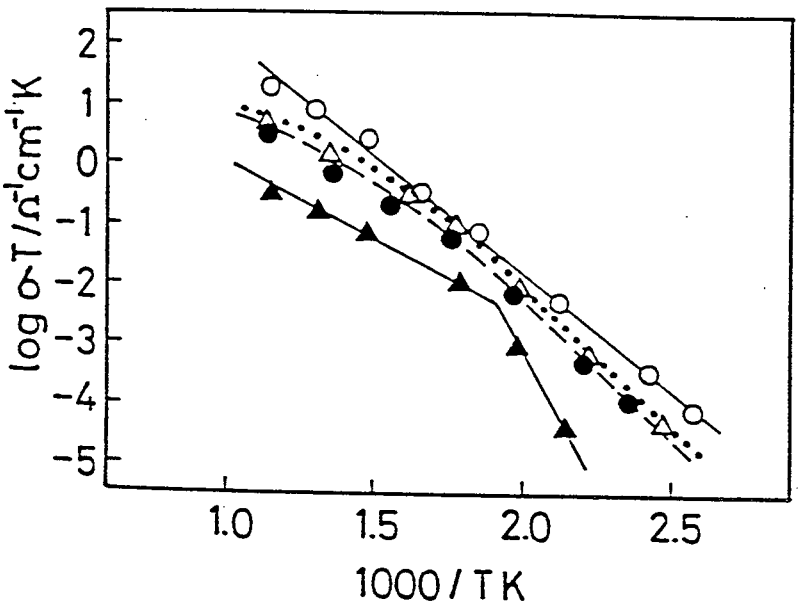

Fig. 7. Temperature dependences of electrical conductivities for Na_2SO_4-$NaVO_3$-$Eu_2(SO_4)_3$ which exhibit phase β.

● Na_2SO_4:$NaVO_3$:$Eu_2(SO_4)_3$=94.6:2.4:3.0

△ Na_2SO_4:$NaVO_3$:$Eu_2(SO_4)_3$=93.2:2.8:4.0

○ Na_2SO_4:$NaVO_3$:$Eu_2(SO_4)_3$=91.0:4.0:5.0

▲ Na_2SO_4

electrical conductivities of this system at a low temperature are much greater than those of Na_2SO_4.

Na_2SO_4-$NaVO_3$-$Pr_2(SO_4)_3$ system

The phases and thermal results of Na_2SO_4 doped with $NaVO_3$ and $Pr_2(SO_4)_3$ are listed in Table 6. From X-ray analysis, the raw materials $NaVO_3$ and $Pr_2(SO_4)_3$ were not detected in all samples. The samples No. 1 and 2 showed the α phase. On the other hand, the samples No. 3, 4, and 5 exhibited the

Table 6. The phases and thermal properties of Na_2SO_4-$NaVO_3$-$Pr_2(SO_4)_3$.

Na_2SO_4 (mol%)	$NaVO_3$ (mol%)	$Pr_2(SO_4)_3$ (mol%)	Phases[a]	DTA peaks[b] (K)
98.0	1.0	1.0	α	493
96.0	2.0	2.0	α	413
94.4	2.6	3.0	β	—
92.8	3.2	4.0	β	—
91.1	3.9	5.0	β	583 (very small)

[a]The α and β phases are similar to the Na_2SO_4-III and Na_2SO_4-I phases, respectively (15, 16). X-ray analyses were done at room temperature.
[b]Reproducibility of DTA temperature is within 8 K.

β phase. In a DTA measurement, the samples that exhibited the β phase show no endothermal peak(the sample No. 3 shows a peak at 587 K, but very small), due to the fact that no phase transformation occurred. Therefore, the samples that exhibited the β phase in Na_2SO_4-$NaVO_3$-$Pr_2(SO_4)_3$ are also good ones for solid electrolytes. The electrical conductivities of Na_2SO_4-$NaVO_3$-$Pr_2(SO_4)_3$ samples which exhibit the β phase are shown in Fig. 8. Electrical conductivities increase about 1.5 orders of magnitude in comparison with Na_2SO_4 and there is no break in the conductivity curve. Cation vacancies increase by doping more $Pr_2(SO_4)_3$. On the other hand, electrical conductivities decrease by doping more $NaVO_3$. These effects cancel each other, the electrical conductivities having almost the same curve in these three samples. The samples of Na_2SO_4-$NaVO_3$-$Pr_2(SO_4)_3$ which exhibit the β phase also keep the structure of the Na_2SO_4-I phase even at a relatively low temperature. Therefore, the electrical conductivities at low temperature are much higher than those of

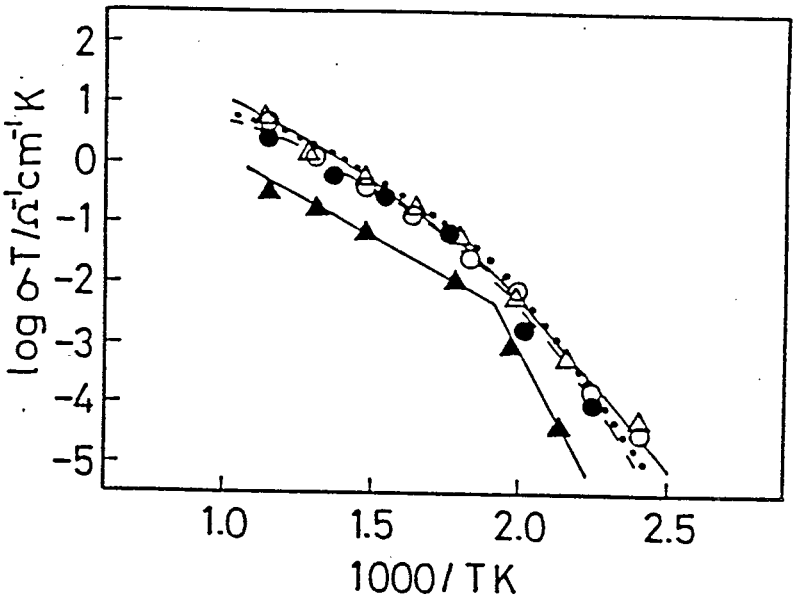

Fig. 8. Temperature dependences of electrical conductivities for Na_2SO_4-$NaVO_3$-$Pr_2(SO_4)_3$ which exhibit phase β.

● Na_2SO_4:$NaVO_3$:$Pr_2(SO_4)_3$=94.4:2.6:3.0

△ Na_2SO_4:$NaVO_3$:$Pr_2(SO_4)_3$=92.8:3.2:4.0

○ Na_2SO_4:$NaVO_3$:$Pr_2(SO_4)_3$=91.1:3.9:5.0

▲ Na_2SO_4

Na_2SO_4.

Na_2SO_4-$NaVO_3$-$Y_2(SO_4)_3$ system

The phases and thermal properties of Na_2SO_4-$NaVO_3$-$Y_2(SO_4)_3$ are presented in Table 7. Samples No. 1 and 2 show phase α which is similar to the phase Na_2SO_4-III. On the other hand, samples NO. 3, 4, and 5 show phase β which resembles the phase Na_2SO_4-I. From DTA analyses, the samples which show phase α exhibit endothermal peaks, that is, a phase transformation still

Table 7. The phases and thermal properties of Na_2SO_4-$NaVO_3$-$Y_2(SO_4)_3$.

Sample No.	Na_2SO_4 (mol%)	$NaVO_3$ (mol%)	$Y_2(SO_4)_3$ (mol%)	Phases	DTA peaks T/K
1	98.3	0.7	1.0	α	485
2	96.9	1.1	2.0	α	408, 463
3	95.7	1.3	3.0	β	—
4	93.6	2.4	4.0	β	—
5	91.4	3.6	5.0	β	573 (very small)

α phase is similar to phase Na_2SO_4-III.[18,19] β phase is similar to phase Na_2SO_4-I.[18,19]

remains. The samples which exhibit phase β show no endothermal peak, indicating that no phase transformation occurs.

The plots of $\log(\sigma T)$ vs. $1/T$ for sodium sulfate doped with $NaVO_3$ and $Y_2(SO_4)_3$(phase β) are given in Fig. 9. The slope of the Na_2SO_4-$NaVO_3$-$Y_2(SO_4)_3$ curves closely approaches to that of Na_2SO_4-I(a high temperature phase). The electrical conductivity of Na_2SO_4-$NaVO_3$-$Y_2(SO_4)_3$ systems is increased with doping $Y_2(SO_4)_3$ because of the increase in cation vacancies. In addition, the Na_2SO_4-$NaVO_3$-$Y_2(SO_4)_3$ systems maintain a Na_2SO_4-I-like phase (phase β) which is excellent in Na^+ ion conduction.

As mentioned above, the conductivity of Na_2SO_4-I is considerably high and the three component systems also support the similar structure with the Na_2SO_4-I phase. Therefore, the conductivity of the solid solution is also high. The Na_2SO_4-$NaVO_3$-$Y_2(SO_4)_3$ systems are considered to

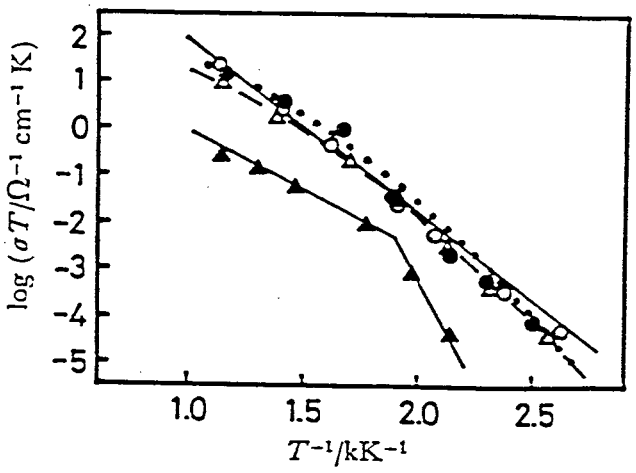

Fig. 9. Temperature dependences of electical conductivities for Na_2SO_4-$NaVO_3$-$Y_2(SO_4)_3$ which exhibit phase β.

△ Na_2SO_4:$NaVO_3$:$Y_2(SO_4)_3$=95.7:1.3:3.0

● Na_2SO_4:$NaVO_3$:$Y_2(SO_4)_3$=93.6:2.4:4.0

○ Na_2SO_4:$NaVO_3$:$Y_2(SO_4)_3$=91.4:3.6:5.0

▲ Na_2SO_4

be very good ionic conductors. In this system, sodium sulfate doped with 3.6 mol% $NaVO_3$ and 5.0 mol% $Y_2(SO_4)_3$ shows the best linearity in the three log(σT)-1/T curves. The three component systems, Na_2SO_4-$NaVO_3$-$Ln_2(SO_4)_3$(Ln=Eu, Pr, Y) solid electrolytes give the optimum composition of 91:4:5.

EMF measurements.

The EMF measurements were performed with Na_2SO_4-$NaVO_3$-$Ln_2(SO_4)_3$ (Ln=Eu, Pr, and Y)(91:4:5) as solid electrolytes. Temperature dependences of measured EMF/calculated EMF ratio with a fixed SO_2 gas concentration are shown in Fig. 10.

The measured EMF for pure Na_2SO_4 and Na_2SO_4-$Ln_2(SO_4)_3$(Ln=

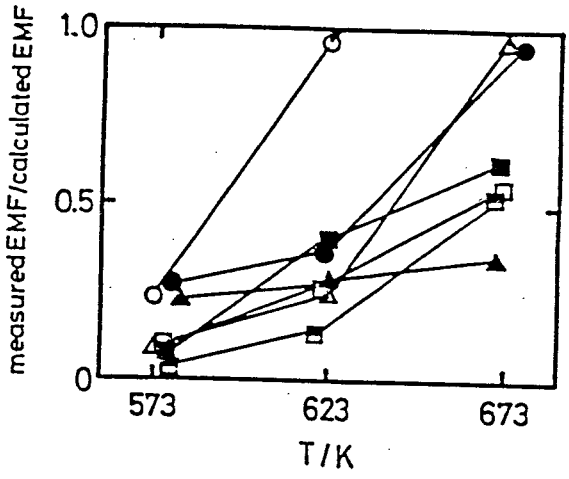

Fig. 10. The ratio of measured EMF/calculated EMF for Na_2SO_4, Na_2SO_4-$Ln_2(SO_4)_3$, Na_2SO_4-$NaVO_3$-$Ln_2(SO_4)_3$(Ln=Eu, Pr, and Y) with inlet SO_2 gas composition, approximately 24 and 8 vol%.

○ Na_2SO_4:$NaVO_3$:$Eu_2(SO_4)_3$=91.0:4.0:5.0

● Na_2SO_4:$NaVO_3$:$Pr_2(SO_4)_3$=91.1:3.9:5.0

△ Na_2SO_4:$NaVO_3$:$Y_2(SO_4)_3$ =91.4:3.6:5.0

□ Na_2SO_4:$Eu_2(SO_4)_3$=95.9:4.1

■ Na_2SO_4:$Pr_2(SO_4)_3$=95.2:4.8

▬ Na_2SO_4:$Y_2(SO_4)_3$ =95.0:5.0

▲ Na_2SO_4

Eu, Pr, and Y) solid solutions were approximately half the value of the calculated EMF[3]. The measured value for sodium sulfate doped with 4.0 mol% $NaVO_3$ and 5.0 mol% $Eu_2(SO_4)_3$ is consistent with that calculated at 623 K and appears to be an appropriate electrolyte. However, the measured value of the EMF has exceeded that calculated at 673 K. This appears to have resulted because Eu^{3+} ions in the systems are easily reduced to a divalent state with SO_2 gas and change in free energies for the reduction might have been added to the

calculated EMF value. Thus, the solid solution of Na_2SO_4-$NaVO_3$-$Eu_2(SO_4)_3$ is not appropriate for the electrolyte.

The systems of Na_2SO_4-$NaVO_3$-$Ln_2(SO_4)_3$(Ln=Pr and Y) give almost the same EMF as calculated one at 673 K. In the temperature range higher than 673 K, the electrolytes became soft because of $NaVO_3$. The EMF measurements in variation of the test SO_2 gas concentration were conducted with the Na_2SO_4-$NaVO_3$-$Ln_2(SO_4)_3$(Ln=Pr and Y) systems as solid electrolytes at 673 K. Results of the EMF measurements with the Na_2SO_4-$NaVO_3$-$Pr_2(SO_4)_3$ electrolyte are presented in Fig. 11. The measured EMF shows good accordance with the calculation

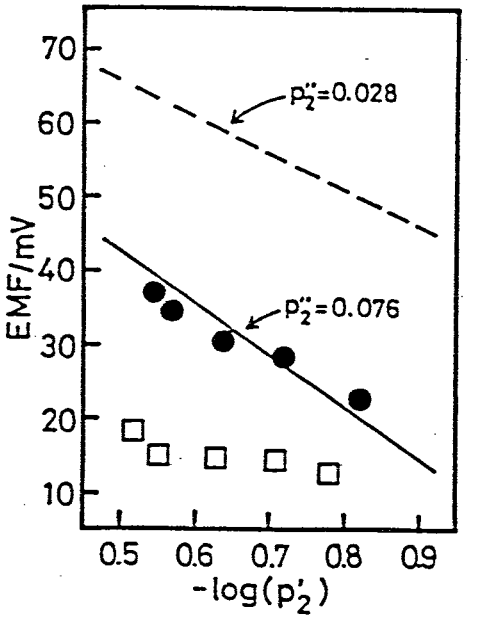

Fig. 11. Variation of the EMF for the concentration cell; Pt$|O_2(p_1')$, $SO_2(p_2')|Na_2SO_4$(3.9 mol% $NaVO_3$, 5.0 mol% $Pr_2(SO_4)_3)|O_2(p_1'')$, $SO_2(p_2'')|$Pt, with p_1''=0.924, p_2''=0.076(●) and p_1''=0.972, p_2''=0.028(□) at 673 K.

—— and — — are calculated EMF[3], respectively.

in which the inlet reference SO_2 gas concentration is 7.6 %. Sodium sulfate doped with $NaVO_3$ and $Pr_2(SO_4)_3$ is able to use for a solid electrolyte, a temperature as low as 673 K which is approximately 300 K lower than pure sodium sulfate can be operative. In the case that the inlet reference SO_2 gas concentration is 2.8 %, the measured EMF is appreciably smaller than the calculated EMF. The EMF results for the Na_2SO_4-$NaVO_3$-$Y_2(SO_4)_3$ electrolyte are also presented in Fig. 12. The measured EMF also shows good agreement with the calculated EMF if the inlet reference SO_2 gas concentration is 8.4 %. The difference between the measured and the calculated EMF also becomes larger when the inlet reference SO_2 gas concentration is 3.6 %.

Dependence of the inlet reference SO_2 gas concentration on the measured EMF/calculated EMF ratios at 673 K for the Na_2SO_4-$NaVO_3$-$Ln_2(SO_4)_3$(Ln=Pr and Y) electrolytes are shown in Fig. 13. The measured EMF/calculated EMF ratio abruptly decreases when the inlet reference SO_2 gas concentration becomes less than 5 %. The gas penetration through the Au-ring might have been happened and resulted in the decrease in EMF values. Furthermore, the electrolyte can not detect SO_2 gas accurately because the SO_2 gas concentration on the surface for the reference electrode is smaller than 5 % and the electrical conductivity of the electrolyte is appreciably low because the operating temperature is as low as 673 K.

A typical EMF response for the Na_2SO_4-$NaVO_3$-$Y_2(SO_4)_3$ electrolyte at 673 K is presented in Fig. 14. The EMF increases immediately when the test SO_2 gas reaches the

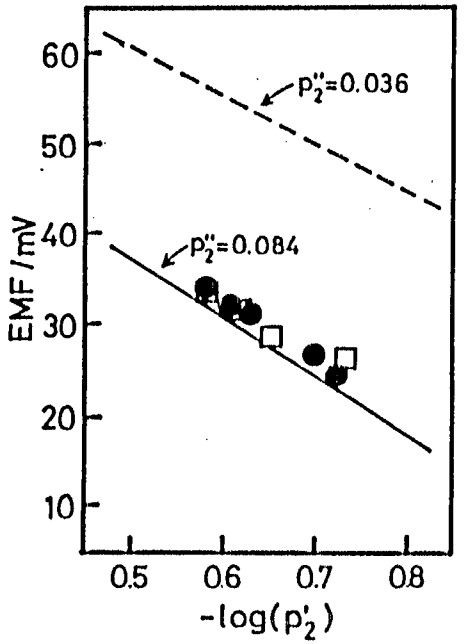

Fig. 12. Variation of the EMF for the concentration cell; Pt$|O_2(p_1')$, $SO_2(p_2')|Na_2SO_4$(3.6 mol% $NaVO_3$, 5.0 mol% $Y_2(SO_4)_3$)$|O_2(p_1'')$, $SO_2(p_2'')|$Pt, with p_1''=0.916, p_2''=0.084(●) and p_1''=0.964, p_2''=0.036(□) at 673 K.

—— and — — are calculated EMF [3], respectively.

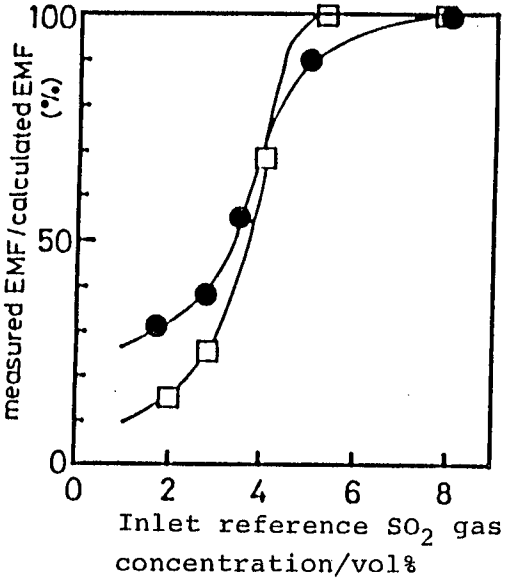

Fig. 13. Dependences of inlet SO_2 gas concentration for reference on measured EMF/calculated EMF at 673 K.

□ Na_2SO_4:$NaVO_3$:$Pr_2(SO_4)_3$=91.1:3.9:5.0

● Na_2SO_4:$NaVO_3$:$Y_2(SO_4)_3$ =91.4:3.6:5.0

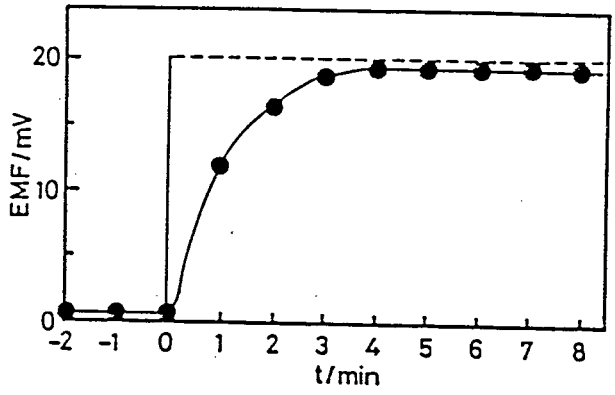

Fig. 14. A typical EMF response for the Na_2SO_4-$NaVO_3$-$Y_2(SO_4)_3$(91.4:3.6:5.0) electrolyte at 673 K. The test and the reference SO_2 gas concentration are 20.5 and 9.7 vol%, respectively.

—·— is calculated EMF[3].

surface of the electrolyte. However, about 4 min are necessary for the EMF to attain 96 % of the calculated EMF. Jacob et al[3] have described that approximately 4 min are required to attain 98 % of the calculated EMF when pure sodium sulfate is used as a solid electrolyte at 973 K. The response time in our measurement coincides with their results. However, operating temperature of ours is approximately 300 K lower than theirs.

2-4. Summary

Sodium sulfate doped with sodium vanadate and rare earth sulfates(Ln=Eu, Pr, and Y) shows higher electrical conductivity for Na^+ ions and maintains a high temperature phase, Na_2SO_4-I, without showing phase transformation. The electromotive force(EMF) using solid solutions, Na_2SO_4-$NaVO_3$-

$Ln_2(SO_4)_3$(Ln= Pr and Y), as solid electrolytes exhibits good agreement with the calculated value, the temperature as low as 673 K which is approximately 300 K lower than pure sodium sulfate can be.

3. THE ELECTRICAL AND THERMAL PROPERTIES OF SODIUM SULFATE MIXED WITH RARE EARTH SULFATES(Ln=Y, Gd) AND SILICON DIOXIDE

3-1. Introduction

In Chapter 2, the solid electrolyte which is applicable at low temperature such as 400^{o}C. The object of this chapter is to develop the appropriate solid electrolyte that is able to be utilized at 700^{o}C. Sodium sulfate was mixed with rare earth sulfates and silicon dioxide so as to enhance the electrical conductivity and to prevent the electrolyte from becoming ductile and also facilitate the sintering.

3-2. Experimental

Materials. Sodium sulfate(purity 99.99 %) and silicon dioxide (purity 99.9 %) were purchased from Wako Pure Chemical Industries Ltd.. Yttrium(purity 99.9 %) and gadolinium oxide(purity 99.99 %) were bought from Shiga Rare Metal Industries Ltd.. Yttrium and gadolinium sulfate were prepared by adding concd. sulfuric acid into Y_2O_3 and Gd_2O_3, respectively. Mixtures of Na_2SO_4-SiO_2, Na_2SO_4-$Ln_2(SO_4)_3$-SiO_2(Ln=Y and Gd) were melted at 1473 K in air, then quenched in air. The resulting sample was pulverized in an agate ball, made into pellets under hydrostatic pressure (2.65×10^8 Pa) and then heated at 1073 K for 1 h in air.

Measurements. X-ray and thermal analyses were performed for the Na_2SO_4-SiO_2 and Na_2SO_4-$Ln_2(SO_4)_3$-SiO_2(Ln=Y and Gd) systems in order to investigate their phases and phase transformations. Electrical conductivities were also measured. EMF measurements were carried out by constructing the SO_2 gas concentration cell depicted in Fig. 15 with a Takeda Riken Digital Multimeter TR-6841. Mixture gases of SO_2 ranging from 6% to 23% were prepared by controlling the SO_2 and the O_2 gas flow volumes with self-made flow meters. The SO_2 gas concentration between 40 ppm and 11100 ppm was regulated by Standard Gas Generator(SGGU-711SD) from Standard Technology Co.. The test SO_2 and O_2 gas mixture is introduced from the tube A depicted in Fig. 15. A Pt net is inserted so as to accelerate the oxidation from SO_2 to SO_3. The gas is led

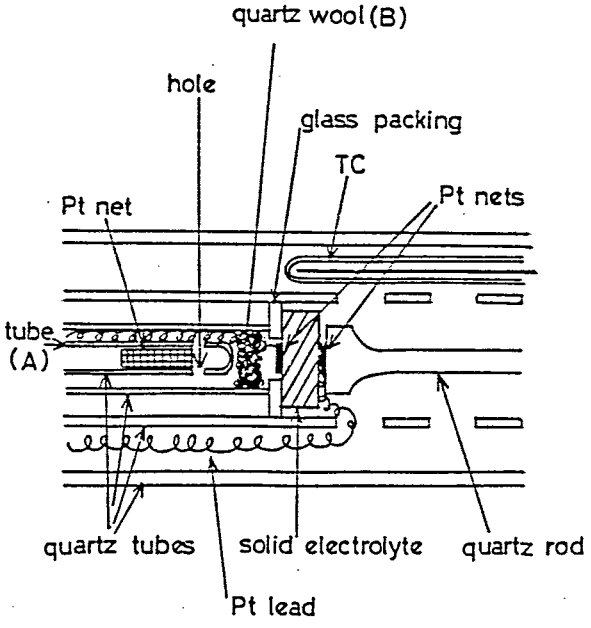

Fig. 15. The apparatus for the electromotive force(EMF) measurements.

to the outer tube compartment through two small holes, and then reaches the electrolyte. The quartz wool is sacked in the place indicated by B shown in Fig. 15 in order to help to diffuse the gas uniformly and to avoid the occurrence of temperature gradient on the electrolyte surface. The ringed glass packing is fixed between the outer quartz tube of the test gas and the solid electrolyte by a spring loading a quartz rod so as to assure the separation of the test gas from the reference gas. The volume of the compartment for the reference SO_2 and O_2 gas mixture has been designed considerably larger compared with that for the test gas so that the SO_2-SO_3 equilibrium can be easily achieved.

3-3. Results and Discussion

Electrical conductivity, phases, and thermal properties.

Na_2SO_4-SiO_2 systems: Na_2SO_4-SiO_2 systems prepared are listed in Table 8 together with the results of X-ray and thermal analyses. All samples show the Na_2SO_4-III phase along with SiO_2. DTA curves also indicate a typical peak of the phase transformation from Na_2SO_4-III to Na_2SO_4-I at

Table 8. The phases and thermal properties of Na_2SO_4-SiO_2.

Sample No.	Na_2SO_4 (mol%)	SiO_2 (mol%)	Phases	DTA peak T/K
1	90	10	Na_2SO_4-III+SiO_2	513
2	70	30	Na_2SO_4-III+SiO_2	513
3	50	50	Na_2SO_4-III+SiO_2	513

513 K. Addition of silicon dioxide to sodium sulfate does not contribute to obtain the Na_2SO_4-I-like phase which is excellent in the Na^+ ion conduction.

Electrical conductivity measurements for Na_2SO_4-SiO_2 system are shown in Fig. 16. Mixing SiO_2 with Na_2SO_4 does not enhance the electrical conductivity. The discontinuity in the log(σT)-1/T curve which is attributed to the III to I phase transformation, also exists for the Na_2SO_4-SiO_2 systems. The temperature at the break is about 513 K, which exactly coincides with the temperature obtained by the DTA measurements. The Na_2SO_4-SiO_2 systems, therefore, do not seem

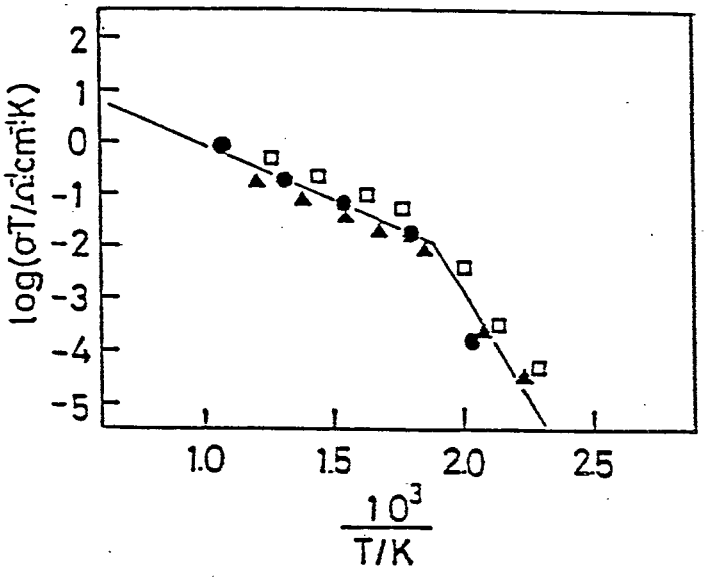

Fig. 16. Temperature dependences of electrical conductivities for the Na_2SO_4-SiO_2

● Na_2SO_4:SiO_2=90:10

□ Na_2SO_4:SiO_2=70:30

▲ Na_2SO_4:SiO_2=50:50

— Na_2SO_4

to be suitable for solid electrolytes because of their low electrical conductivities and because of the existence of the phase transformation from III to I.

Na_2SO_4-$Y_2(SO_4)_3$-SiO_2 systems: The results of phase analyses and DTA measurements are presented in Table 9. X-ray measurements indicate that a new phase, A, in which the peaks of Na_2SO_4-I-like phase is included, and a small amount of SiO_2 coexists. In sample NO.1, some peaks of phase A split. Therefore, a symbol A' is given to this phase instead of A. This sample(NO.1) exhibits an endothermal peak with no gravimetric change at 593 K, showing that a phase transformation occurs. On the other hand, samples from NO.2 to 5 exhibit no phase transition.

Figure 17 illustrates the electrical conductivities results for Na_2SO_4-$Y_2(SO_4)_3$-SiO_2 systems. Sample NO.1 exhibits relatively high conductivity. However, the discontinuity lies in the $\log(\sigma T)$ vs. $1/T$ curve approximately at 593 K. This temperature is identical with the results from DTA measurement. Similar $\log(\sigma T)$-$1/T$ curves were obtained for the samples of NO. 2, 3, and 4. Their curves are nearly straight lines and their conductivities are about 20 times larger than that of Na_2SO_4 at 873 K. In the case of 14.8 mol% $Y_2(SO_4)_3$(NO. 5), the electrical conductivity decreased. The cation vacancies are apt to form clusters which do not contribute to the cation conduction.

In the system of Na_2SO_4-$Y_2(SO_4)_3$-SiO_2, the samples from NO. 2 to 4 can be applied as solid electrolytes for an SO_2 gas detector.

Table 9. The phases and thermal properties of Na_2SO_4-$Y_2(SO_4)_3$-SiO_2

sample NO.	Na_2SO_4 (mol%)	$Y_2(SO_4)_3$ (mol%)	SiO_2 (mol%)	phases	DTA peak (°C)
1	55.1	4.9	40.0	A'+(small SiO_2)	320
2	52.2	7.7	40.1	A+(small SiO_2)	——
3	50.1	9.9	40.0	A+(small SiO_2)	——
4	48.1	11.8	40.1	A+(small SiO_2)	——
5	45.1	14.8	40.1	A+(small SiO_2)	——

A and A' : the phases which include the peaks of Na_2SO_4-I-like phase

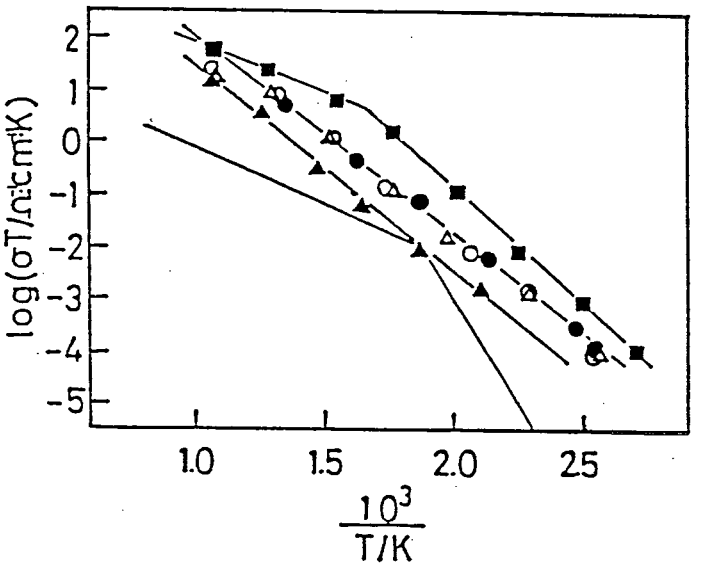

Fig. 17. Temperature dependences of electrical conductivities for the Na_2SO_4-$Y_2(SO_4)_3$-SiO_2.

■ Na_2SO_4:$Y_2(SO_4)_3$;SiO_2=55.1: 4.9:40.0

○ Na_2SO_4:$Y_2(SO_4)_3$:SiO_2=52.2: 7.7:40.1

● Na_2SO_4:$Y_2(SO_4)_3$:SiO_2=50.1: 9.9:40.0

△ Na_2SO_4:$Y_2(SO_4)_3$:SiO_2=48.1:11.8:40.1

▲ Na_2SO_4:$Y_2(SO_4)_3$:SiO_2=45.1:14.8:40.1

— Na_2SO_4

Na_2SO_4-$Gd_2(SO_4)_3$-SiO_2 systems: The phases and thermal properties of Na_2SO_4-$Gd_2(SO_4)_3$-SiO_2 system are tabulated in Table 10. The samples NO. 1 to NO. 4 exhibit a new phase α with a small amount of SiO_2. This phase is the phase where some peaks of phase A, are disappearing. The peaks of phase α' are slightly deviated from those of phase α toward low degree side except a peak at 31.6 degree. From thermal analyses, every sample exhibits no endo- or exothermal peak on its DTA curve. The results of electrical conductivities for

Table 10. The phases and thermal properties of Na_2SO_4-$Gd_2(SO_4)_3$-SiO_2

sample NO.	Na_2SO_4 (mol%)	$Gd_2(SO_4)_3$ (mol%)	SiO_2 (mol%)	phases	DTA peak (°C)
1	55.2	4.7	40.1	α+(small SiO_2)	——
2	52.0	8.0	40.0	α+(small SiO_2)	——
3	51.0	8.2	40.8	α+(small SiO_2)	——
4	48.2	11.6	40.2	α+(small SiO_2)	——
5	43.8	17.2	39.0	α'+(small SiO_2)	——

α and α': the phases which include the peaks of Na_2SO_4-I-like phase

Na_2SO_4-$Gd_2(SO_4)_3$-SiO_2 systems are presented in Fig. 18. The electrical conductivities for the sample NO. 1-3 show the highest values in the systems(at temperature higher than 781 K). In the case of 11.6mol% $Gd_2(SO_4)_3$, its conductivity decreased. This is because of the formation of cation vacancy clusters. When 17.2 mol% of $Gd_2(SO_4)_3$ is added(NO. 5), the electrical conductivities become higher even at low temperatures. However, the bend in log(σT) vs. 1/T curve appears at approximately 543 K.

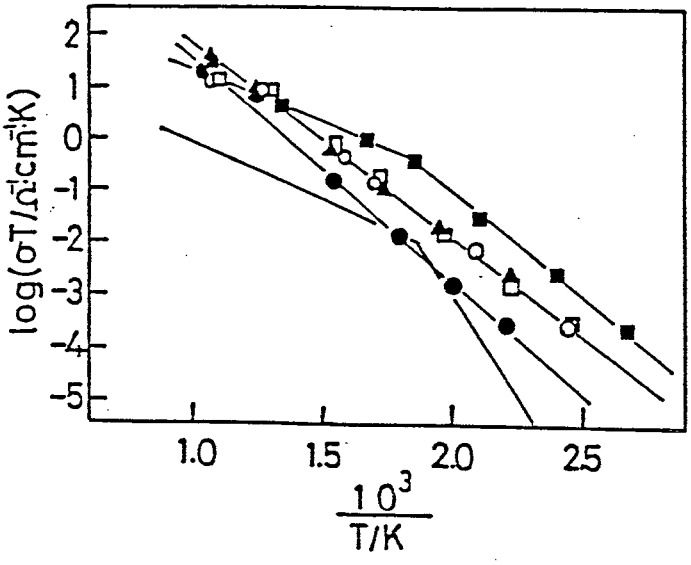

Fig. 18. Temperature dependences of electrical conductivities for the Na_2SO_4-$Gd_2(SO_4)_3$-SiO_2

□ Na_2SO_4:$Gd_2(SO_4)_3$:SiO_2=55.2: 4.7:40.1

○ Na_2SO_4:$Gd_2(SO_4)_3$:SiO_2=52.0: 8.0:40.0

▲ Na_2SO_4:$Gd_2(SO_4)_3$:SiO_2=51.0: 8.2:40.8

● Na_2SO_4:$Gd_2(SO_4)_3$:SiO_2=48.2:11.6:40.2

■ Na_2SO_4:$Gd_2(SO_4)_3$:SiO_2=43.8:17.2:39.0

— Na_2SO_4

In the Na_2SO_4-$Gd_2(SO_4)_3$-SiO_2 systems, the samples NO. 1-3 are good candidates for solid electrolytes.

EMF measurements.

EMF measurements with the appropriate sample of Na_2SO_4-$Y_2(SO_4)_3$-SiO_2(50.1:9.9:40.0) are shown in Fig. 19. The measured EMF was in good agreement with the calculated EMF, with the inlet SO_2 gas concentration between 0.1 % (1000 ppm) and 23 %. When the inlet SO_2 gas concentration was less than 0.1 %, the measured EMF becomes lower than the calculated EMF. Figure 20 presents the variation of the EMF with the pertinent sample of Na_2SO_4-$Gd_2(SO_4)_3$-SiO_2 (51.0:8.2:40.8). The measured EMF coincided with calculated EMF, with the inlet SO_2 gas range from 0.32 %(3200 ppm) to 10 %. When the inlet SO_2 gas content was smaller than 0.32 %, the difference between the measured and the calculated EMF became larger.

Sodium sulfate electrolytes mixed with $Y_2(SO_4)_3$ and SiO_2 can not detect the SO_2 gas less than 1000 ppm(0.1 %). This is attributed to the difficulties in the formation and decomposition of sodium sulfate on the electrolyte surfaces, and in obtaining the suitable contact between the Pt net electrode and the electrolyte. In order to improve the EMF characteristics in the smaller SO_2 gas content range(<1000 ppm), platinum sputtering on the center surface of the electrolyte was attempted.

The platinum sputtering was conducted on the center surface(about 5×10^{-3} m in diameter) of the solid electrolyte

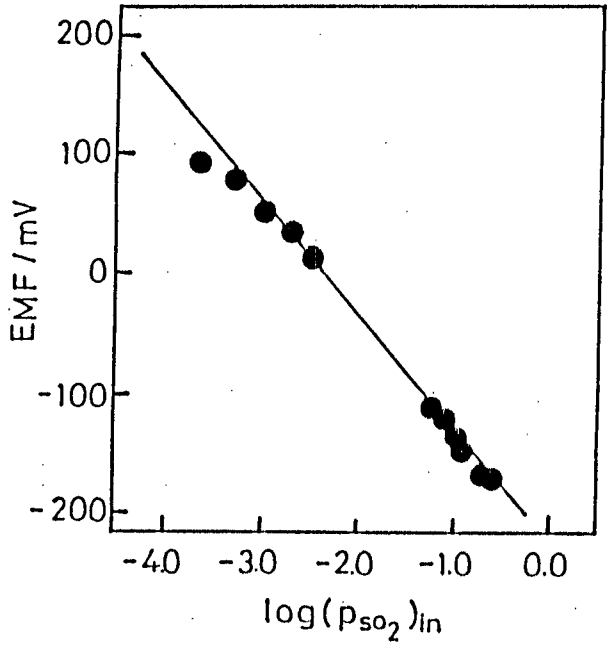

Fig. 19. Variation of the EMF for the concentration cell; Pt$\left|O_2(p_1'), SO_2(p_2')\right|Na_2SO_4$(9.9 mol% $Y_2(SO_4)_3$, 40.0 mol% SiO_2)$\left|O_2(p_1''), SO_2(p_2'')\right|$Pt, with p_1''=0.996 and p_2''=0.004 at 973 K.

——— is calculated EMF[3].

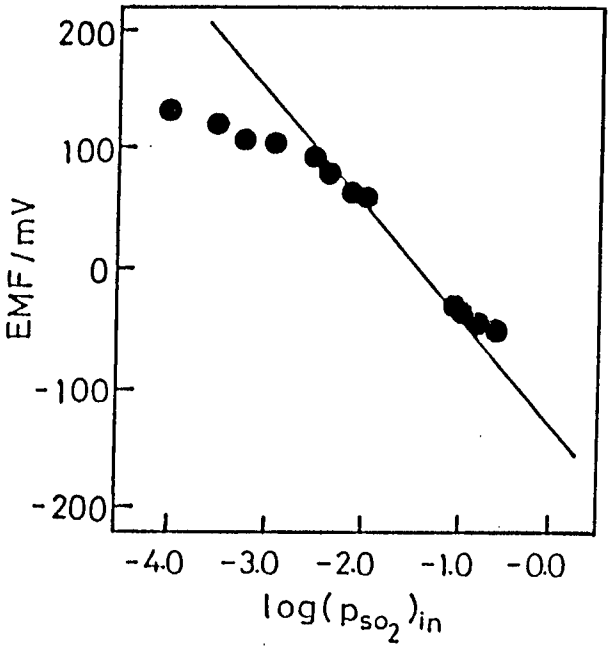

Fig. 20. Variation of the EMF for the concentration cell; Pt$\left|O_2(p_1'), SO_2(p_2')\right|Na_2SO_4$(8.2 mol% $Gd_2(SO_4)_3$, 40.8 mol% SiO_2)$\left|O_2(p_1''), SO_2(p_2'')\right|$Pt, with p_1''=0.966 and p_2''=0.034 at 973 K.

——— is calculated EMF[3].

(1.3×10^{-2} m in diameter) with Shimadzu's Ion Coater IC-50. Approximately 10 nm thickness of the Pt film was obtained by the 10 min Pt sputtering. In the EMF measurements for the electrolyte with Pt sputtering, the reference SO_2 and O_2 gas mixture was regulated with a commercial gas flow meter KOFLOG RK 1200 from Kojima Flow Instruments Co. and Pt mesh was installed instead of the quartz wool(B) as shown in Fig. 21.

Na_2SO_4 systems(Pt sputtering)

Sodium sulfate samples with platinum sputtering for 10 min on working and on both surfaces were prepared. Figure 22 presents the EMF variations together with sodium sulfate without sputtering. The measured EMF was consistent with the calculated EMF in the inlet SO_2 gas concentration

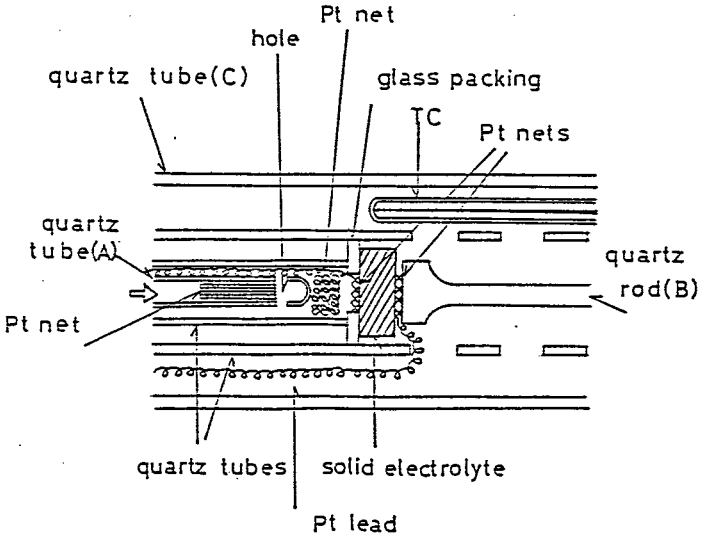

Fig. 21. The apparatus for the EMF measurements.

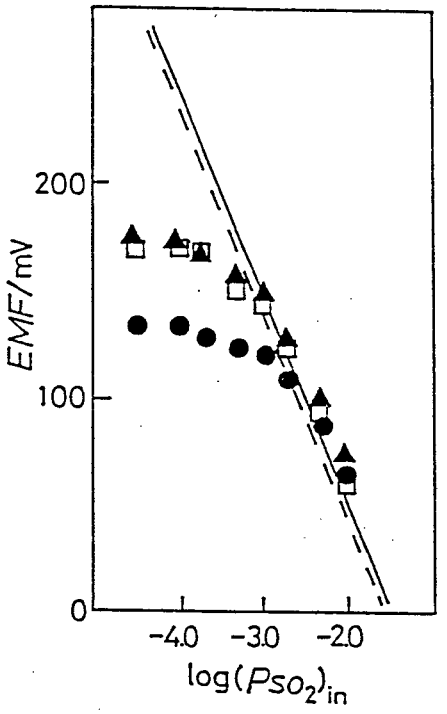

Fig. 22. The variation of the EMF for Na_2SO_4 solid electrolyte with the SO_2 gas concentration

● Na_2SO_4 (without Pt sputtering) (———)

□ Na_2SO_4 (10 min Pt sputtering on working electrode surface only) (— —)

▲ Na_2SO_4 (10 min Pt sputtering on both surfaces) (———)

—— and — — are calculated EMF[3], respectively.

between 0.2 % and 1 %. The measured EMF of the sodium sulfate without Pt sputtering becomes appreciably lower than the calculated value in the $\log(P_{SO_2})_{in}$ expression -2.7(2000 ppm). The EMF characteristics of the Pt sputtered sample were improved in the lower concentration(<0.2 %) compared with that of Na_2SO_4 without sputtering. The suitable contact between the Pt net electrode and the electrolyte can be obtained by the

sputtering. No meaningful difference in the EMF characteristics exists in the two Pt sputtered samples. The difference between the measured and the calculated EMF becomes larger, the SO_2 gas content smaller than 0.1 %($\log(p_{SO_2})_{in}$=-3.0), with Pt sputtered samples. These may result from the permeation of the ambient gases in the electrolyte because of the cracks produced from the III to I phase transformation.

Na_2SO_4-$Y_2(SO_4)_3$-SiO_2 systems(Pt sputtering)

The results of the EMF measurements with various SO_2 gas concentration are presented in Fig. 23. The samples with 5 min Pt sputtering and 10 min sputtering on working electrode side, were prepared in addition to the sample without sputtering. The measured EMF for the Na_2SO_4-$Y_2(SO_4)_3$-SiO_2 without sputtering was in good accordance with the calculated value in the $\log(p_{SO_2})_{in}$ description from -3.0 to -2.0. Compared with the calculated EMF, the measured EMF decreases at an SO_2 gas content smaller than 1000 ppm. 5 min sputtering enables the electrolyte to detect the SO_2 gas adequately from 500 ppm($\log(p_{SO_2})_{in}$= -3.3) to 10000 ppm(1 %). By 10 min sputtering, the further lower SO_2 gas detection limit of 200 ppm($\log(p_{SO_2})_{in}$=-3.7) was observed. The more the platinum sputtering time increases, the closer the measured EMF approaches to the calculated value. The formation and the decomposition of the sodium sulfate on the electrolyte surface come to occur easily by the Pt sputtering. 10, 20, and 30 min Pt sputtered samples on working electrode surface are also exhibited in Fig. 24. There is no significant differences in

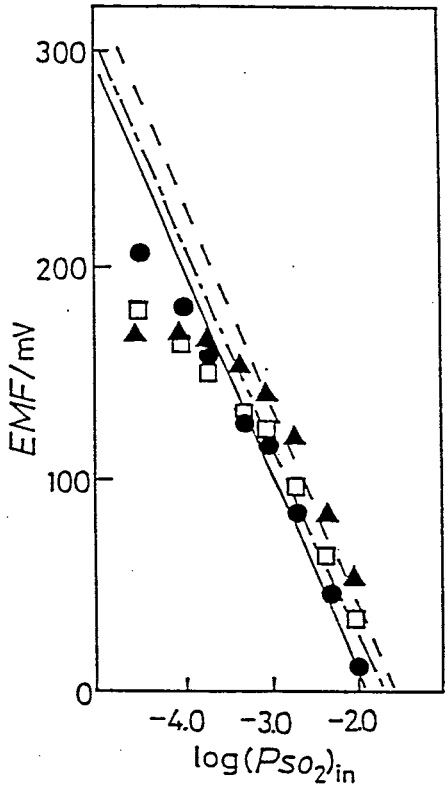

Fig. 23. The variation of the EMF for Na_2SO_4-$Y_2(SO_4)_3$-SiO_2(48.1:11.8:40.1) solid electrolyte with the SO_2 gas concentration(Pt sputtering on working electrode surface only)

▲ Na_2SO_4-$Y_2(SO_4)_3$-SiO_2(0 min) (— — —)

□ Na_2SO_4-$Y_2(SO_4)_3$-SiO_2(5 min) (— — —)

● Na_2SO_4-$Y_2(SO_4)_3$-SiO_2(10 min) (———)

— — —, — — —, and ——— are calculated EMF[3], respectively.

these three samples. Only at 30 ppm($\log(p_{SO_2})_{in}$=-4.52), the electrolyte with 10 min Pt sputtering shows the nearest EMF value to the calculated in these samples. The dependence of the Pt sputtering time on the measured EMF/calculated EMF ratio is shown in Fig. 25. The measured EMF/ calculated EMF proportion

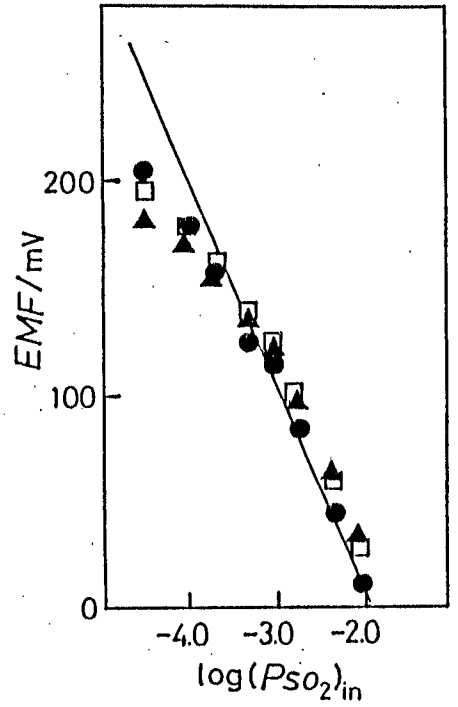

Fig. 24. The variation of the EMF for Na_2SO_4-$Y_2(SO_4)_3$-SiO_2(48.1:11.8:40.1) solid electrolyte with the SO_2 gas concentration (Pt sputtering on working electrode surface only)

- ● Na_2SO_4-$Y_2(SO_4)_3$-SiO_2 (10 min)
- □ Na_2SO_4-$Y_2(SO_4)_3$-SiO_2 (20 min)
- ▲ Na_2SO_4-$Y_2(SO_4)_3$-SiO_2 (30 min)
- —— is calculated EMF[3].

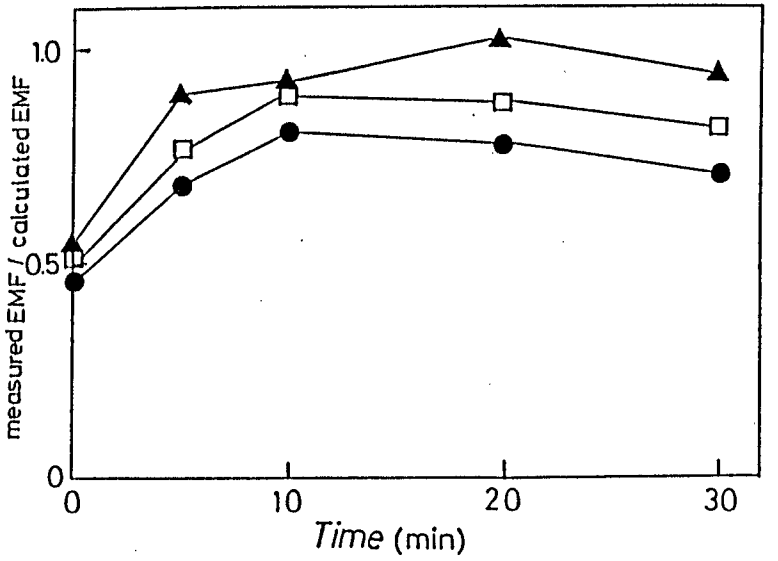

Fig. 25. The Pt sputtering time dependences of measured EMF/calculated EMF with various test SO_2 gas concentration

- ● 30 ppm
- □ 100 ppm
- ▲ 500 ppm

abruptly enhances itself with the increase in the Pt sputtering time up to 10 min. No meaningful differences exist when the Pt sputtering time is more than 10 min. The most appropriate platinum sputtering time is determined to be 10 min. Because the 10 min is good enough to sputter, both surfaces of the electrolyte has been sputtered. The results

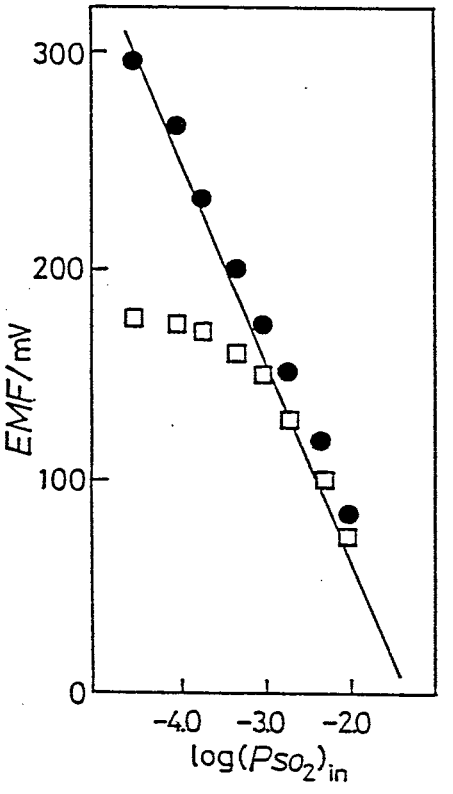

Fig. 26. The variation of the EMF for Na_2SO_4 and Na_2SO_4-$Y_2(SO_4)_3$-SiO_2 solid electrolytes with the SO_2 gas concentration (Pt sputtering on both surfaces for 10 min)

● Na_2SO_4-$Y_2(SO_4)_3$-SiO_2

□ Na_2SO_4

—— is calculated EMF[3].

for Na_2SO_4-$Y_2(SO_4)_3$-SiO_2 solid electrolyte with sputtering on both surfaces are presented in Fig. 26 together with the result of Na_2SO_4. The EMF characteristics for Na_2SO_4 remarkably decrease as a result of the penetration through the cleavage appearing in the electrolyte, the SO_2 gas concentration less than 0.1 %. On the other hand, the measured EMF for the Na_2SO_4-$Y_2(SO_4)_3$-SiO_2 excellently agreed with the calculated EMF from 30 ppm to 1 %.

3-4. Summary

Sodium sulfate mixed with rare earth sulfates(Ln=Y and Gd) and silicon dioxide exhibits a Na_2SO_4-I-like phase as well as a small amount of silicon dioxide phase. The former phase is excellent in Na^+ ion conduction. The electrical conductivity of the Na_2SO_4-$Ln_2(SO_4)_3$-SiO_2(Ln=Y and Gd) systems is considerably higher than that of pure sodium sulfate. When the Na_2SO_4-$Ln_2(SO_4)_3$-SiO_2(Ln=Y and Gd) sample is applied as a solid electrolyte for an SO_2 gas concentration cell, the measured EMF is in good agreement with the calculated EMF for an SO_2 gas concentration range from 0.1 %(1000 ppm) to 23 %, and 0.32 %(3200 ppm) to 10 %, respectively. The platinum sputtering on the center surface of the electrolyte was performed. The Platinum sputtering appreciably contributed to the enhancement of the EMF characteristics for the SO_2 gas content till 30 ppm.

Chapter 4

THE ELECTRICAL AND THERMAL PROPERTIES OF SODIUM SULFATE MIXED WITH RARE EARTH SULFATES(Ln=La, Y) AND ALUMINUM OXIDE

4-1. Indroduction

In Chapter 3, silicon dioxide has been mixed for the purpose of preventing the solid electrolyte from becoming soft and improving the sinterability of the electrolyte. In this chapter, aluminum oxide was mixed instead of silicon dioxide so as to obtain harder and further heat-endurable electrolyte than the silicon dioxide mixed one. Rare earth sulfates are also mixed in order to increase the conductivity. Because the platinum sputtering considerably improved the EMF characteristics, platinum was sputtered on both center surface of the Na_2SO_4-$Ln_2(SO_4)_3$-Al_2O_3 solid electrolyte.

4-2. Experimental

Materials: Sodium sulfate(purity: 99.99 %) and aluminum oxide(purity: 99.98 %) were purchased from Wako Pure Chemical Industries Ltd. Rare earth oxide(purity: 99.99 %) was bought from Shiga Rare Metal Industries Ltd. Rare earth sulfate was

prepared by adding a concentrated sulfuric acid into the rare earth oxide. Sodium sulfate(Na_2SO_4), rare earth sulfates($Ln_2(SO_4)_3$), and aluminum oxide(Al_2O_3) were preheated in a porcelain crucible for dehydration before weighing. The appropriate amount of Na_2SO_4, $Ln_2(SO_4)_3$, and Al_2O_3 was mixed thoroughly in an agate mortar. The mixture of Na_2SO_4-$Ln_2(SO_4)_3$-Al_2O_3 was melted at 1473 K in a platinum crucible in air atmosphere, and then quenched in air. The resultant was ground(<74 μm) and made into pellets in a hydrostatic pressure(2.65×10^8 Pa). The pellets were sintered at 1073 K for 1 h in air and then quenched in air. Platinum powder was sputtered on both center surfaces (5×10^{-3} m in diameter) of the electrolyte(1.3×10^{-2} m in diameter).

measurements: Electrical conductivity and EMF measurements were conducted as described in Chapter 3.

4-3. Results and Discussion

Phases and thermal properties

Na_2SO_4-$La_2(SO_4)_3$-Al_2O_3 system

X-ray and DTA results for Na_2SO_4-$La_2(SO_4)_3$-Al_2O_3 are tabulated in Table 11. All samples show a new phase, A, which is analogous to the Na_2SO_4-I phase, together with aluminum oxide phase. This Na_2SO_4-I phase is effective for Na^+ cationic conduction. Lanthanum aluminate($LaAlO_3$) coexists except for the sample NO. 7. Furthermore, unknown phase, B, exists in the samples from NO. 4 to 7.

Table 11. The phases and thermal properties of Na_2SO_4-$La_2(SO_4)_3$-Al_2O_3

sample NO.	Na_2SO_4 mol%	$La_2(SO_4)_3$ mol%	Al_2O_3 mol%	phases	DTA peak K
1	55.0	5.0	40.0	A+Al_2O_3+$LaAlO_3$(s)	593
2	52.1	7.8	40.1	A+Al_2O_3+$LaAlO_3$	603
3	50.0	10.1	39.9	A+Al_2O_3+$LaAlO_3$	603
4	48.0	12.0	40.0	A+Al_2O_3+$LaAlO_3$+B(s)	603
5	44.8	15.3	39.9	A+Al_2O_3+$LaAlO_3$+B(s)	603
6	42.4	18.1	39.5	A+Al_2O_3+$LaAlO_3$+B	603
7	40.1	19.8	40.1	A+Al_2O_3+B	593

A: Na_2SO_4-I-similar phase, B: unknown phase

(s): small amount

In the DTA measurements, all samples exhibited an endothermal peak at 593 or 603 K. This means that a phase transition occurs. However, the peaks are appreciably small. The doping of $La_2(SO_4)_3$ and Al_2O_3 into sodium sulfate considerably contributes to the suppression of the phase transformation.

Na_2SO_4-$Y_2(SO_4)_3$-Al_2O_3 system

The phases and thermal properties of Na_2SO_4-$Y_2(SO_4)_3$-Al_2O_3 are shown in Table 12. The phase, A, which is similar to Na_2SO_4-I phase, exists along with aluminum oxide phase. Yttrium oxide phase, which has been produced from the decomposition of $Y_2(SO_4)_3$, coexists in all samples. However, the samples No. 3 and 4 exhibit only a trace peak of Y_2O_3 phase. From DTA analyses, No. 3 and 4 show no endothermal peak. This means that the phase transition has been suppressed.

Electrical conductivity measurements

Na_2SO_4-$La_2(SO_4)_3$-Al_2O_3 system

The plots of $\log(\sigma T)$ vs. $1/T$ for the sample NO. 1-3 are shown in Fig. 27. A deflection in the σT vs. $1/T$ curves exists in these samples. This kneel temperature is approximately 603 K, which is almost consistent with the DTA results. All samples show higher electrical conductivity than pure sodium sulfate. The mixing of $La_2(SO_4)_3$ into sodium sulfate makes more effective cation vacancies for ionic migration because of the electroneutralization.

Table 12. The phases and thermal properties of Na_2SO_4-$Y_2(SO_4)_3$-Al_2O_3

Na_2SO_4 (mol%)	$Y_2(SO_4)_3$ (mol%)	Al_2O_3 (mol%)	phases	DTA peaks (^oC)
55	5	40	A+Al_2O_3+Y_2O_3(t)	210, 285
52	8	40	A+Al_2O_3+Y_2O_3	235, 280
50	10	40	A+Al_2O_3+Y_2O_3(t)	———
48	12	40	A+Al_2O_3+Y_2O_3(t)	———
45	15	40	A+Al_2O_3+Y_2O_3	230, 285
43	17	40	A+Al_2O_3+Y_2O_3	225, 285
40	20	40	A+Al_2O_3+Y_2O_3	235, 285

A: Na_2SO_4-I-similar phase

(t): trace

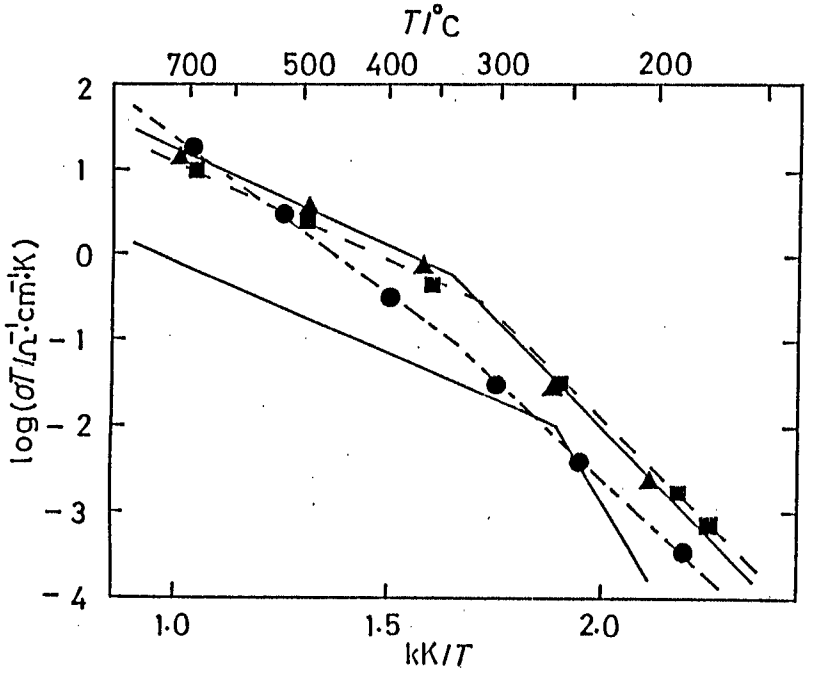

Fig. 27. Temperature dependences of electrical conductivities for Na_2SO_4-$La_2(SO_4)_3$-Al_2O_3

- Na_2SO_4:$La_2(SO_4)_3$:Al_2O_3 = 55.0: 5.0:40.0
- Na_2SO_4:$La_2(SO_4)_3$:Al_2O_3 = 52.1: 7.8:40.1
- Na_2SO_4:$La_2(SO_4)_3$:Al_2O_3 = 50.0:10.1:39.9
- Na_2SO_4

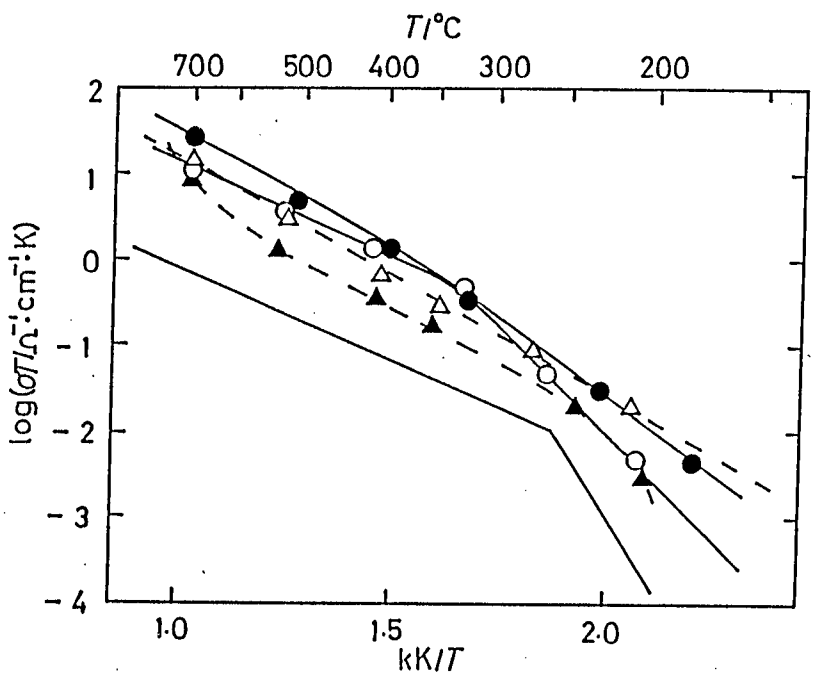

Fig. 28. Temperature dependences of electrical conductivities for Na_2SO_4-$La_2(SO_4)_3$-Al_2O_3

- Na_2SO_4:$La_2(SO_4)_3$:Al_2O_3 = 48.0:12.0:40.0
- Na_2SO_4:$La_2(SO_4)_3$:Al_2O_3 = 44.8:15.3:39.9
- Na_2SO_4:$La_2(SO_4)_3$:Al_2O_3 = 42.4:18.1:39.5
- Na_2SO_4:$La_2(SO_4)_3$:Al_2O_3 = 40.1:19.8:40.1
- Na_2SO_4

Figure 28 presents the electrical conductivity results for the sample NO.4-7. The bend in the curve also occurs in NO. 4. This deflection temperature at about 603 K is identical to the temperature at DTA peak. The curves for the Na_2SO_4-$La_2(SO_4)_3$-Al_2O_3, of which $La_2(SO_4)_3$ has been mixed more than 15.3 mol %, show almost straight in the σT vs. 1/T relation. The highest σT value was obtained in the sample NO. 5. The cation vacancies begin to make clusters which do not contribute to the cation conduction by the mixing of $La_2(SO_4)_3$ more than 18.1 mol %.

From these results, the most appropriate sample for the solid electrolyte for a sulfur dioxide gas detector is found to be the sample NO. 5.

Na_2SO_4-$Y_2(SO_4)_3$-Al_2O_3 system

The electrical conductivity results for the sample No. 1 and 2 are presented in Fig. 29. Both samples exhibit slightly higher conductivity compared with pure sodium sulfate. However, the discontinuity in the $\log(\sigma T)$-1/T curves exists by the phase transformation. The $\log(\sigma T)$ vs. 1/T relation for the samples No. 3 and 4 is appeared in Fig. 30. The conductivity considerably enhanced in comparison with the samples No. 1 and 2. This may be attributed to the fact that the cation vacancies which have been produced by the $Y_2(SO_4)_3$ doping, increase. The σT vs. 1/T curves for the samples No. 5, 6, and 7 are presented in Fig. 31. The conductivity decreases and the break in the curves appears again. The decrease in the conductivity is ascribed to the formation of cation clusters.

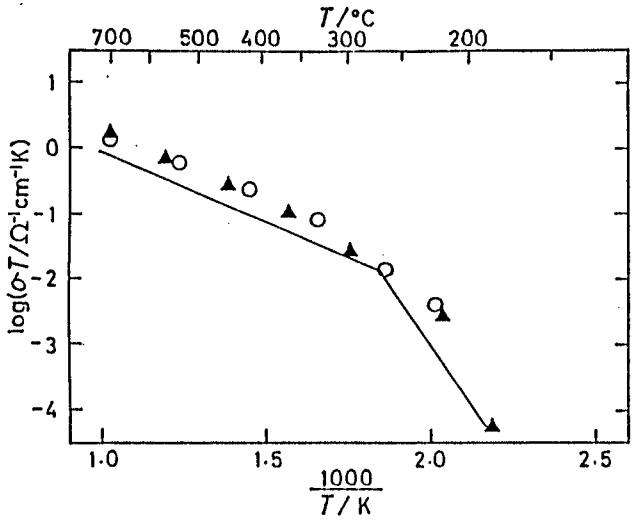

Fig. 29. Temperature dependences of electrical conductivities for Na_2SO_4-$Y_2(SO_4)_3$-Al_2O_3

○ Na_2SO_4:$Y_2(SO_4)_3$:Al_2O_3=55: 5:40

▲ Na_2SO_4:$Y_2(SO_4)_3$:Al_2O_3=52: 8:40

—— Na_2SO_4

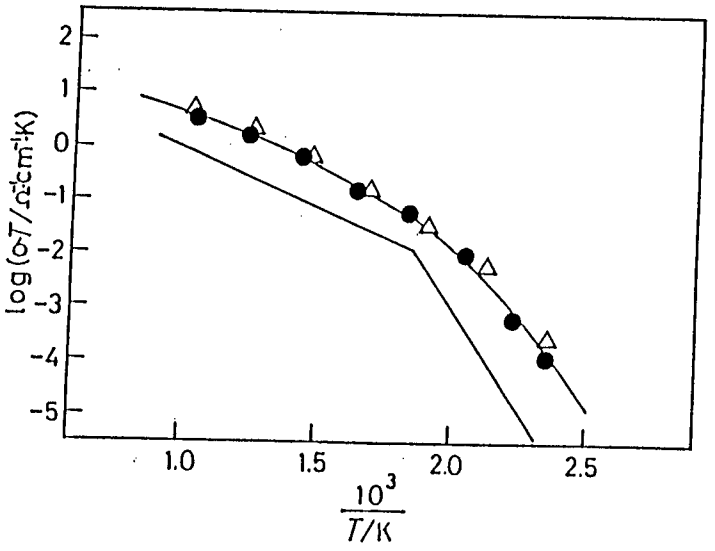

Fig. 30. Temperature dependences of electrical conductivities for Na_2SO_4-$Y_2(SO_4)_3$-Al_2O_3.

● Na_2SO_4:$Y_2(SO_4)_3$:Al_2O_3=50:10:40

△ Na_2SO_4:$Y_2(SO_4)_3$:Al_2O_3=48:12:40

—— Na_2SO_4

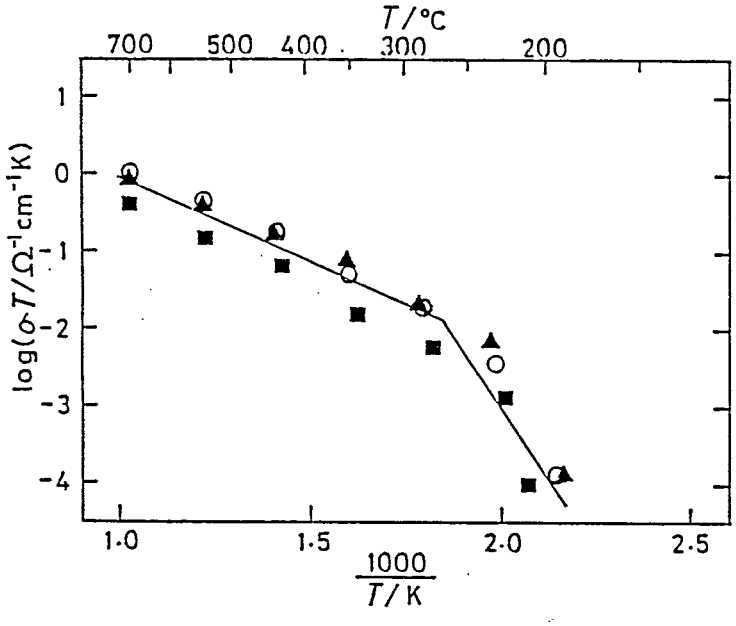

Fig. 31. Temperature dependences of electrical conductivities for Na_2SO_4-$Y_2(SO_4)_3$-Al_2O_3.

○ Na_2SO_4:$Y_2(SO_4)_3$;Al_2O_3=45:15:40

▲ Na_2SO_4:$Y_2(SO_4)_3$:Al_2O_3=43:17:40

■ Na_2SO_4:$Y_2(SO_4)_3$:Al_2O_3=40:20:40

— Na_2SO_4

These results mean that the proper solid electrolyte in Na_2SO_4-$Y_2(SO_4)_3$-Al_2O_3 system is determined to the samples No. 3 and 4.

EMF measurements

The variation of the EMF for the Na_2SO_4-$La_2(SO_4)_3$-Al_2O_3 (NO.5) at 973 K is shown in Fig. 32. The inlet SO_2 gas concentration was varied from 30 ppm($\log(p_{SO_2})_{in}$=-4.52) to 1 %($\log(p_{SO_2})_{in}$=-2.0), while the reference inlet SO_2 gas content was fixed at approximately 3 % by sulfur dioxide and oxygen gas mixing. The measured EMF was in good agreement with the

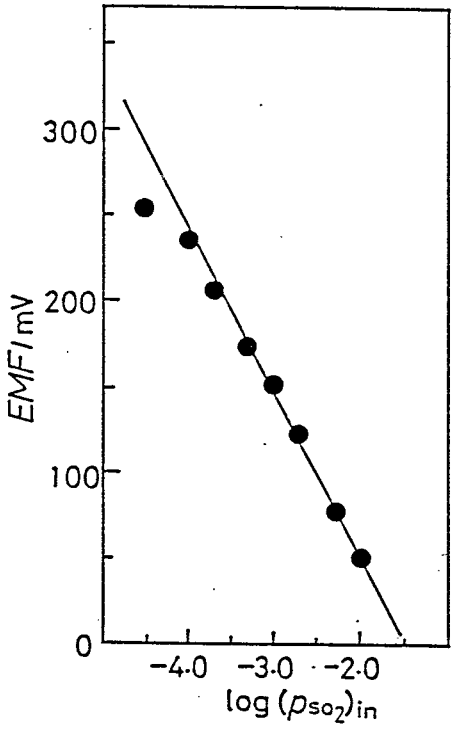

Fig. 32. The variation of the EMF for Na_2SO_4-$La_2(SO_4)_3$-Al_2O_3(44.8:15.3:39.9) solid electrolyte at 973 K.

———— calculated EMF[3].

calculated EMF, in the inlet SO_2 gas concentration from 100 ppm($\log(p_{SO_2})_{in}$=-4.0) to 1 %. The difference between the measured and calculated EMF was almost 40 mV at 30 ppm. This may be attributed to the fact that the gas permeation occurs through the microcracks which have been resulted from the phase transition.

4-4. Summary

Sodium sulfate mixed with rare earth sulfate and aluminum oxide was prepared and its phases and electrical properties were investigated. The Na_2SO_4-$Ln_2(SO_4)_3$-Al_2O_3 sample maintains a Na_2SO_4-I-similar phase and exhibits higher electrical conductivity compared with unmixed sodium sulfate.

Electromotive force(EMF) measurements were carried out by constructing the sulfur oxides concentration cell. The measured EMF was in good agreement with the calculated EMF, in the inlet SO_2 gas concentration from 100 ppm to 1 %.

Chapter 5

THE ELECTRICAL AND THERMAL PROPERTIES OF SODIUM SULFATE MIXED WITH LITHIUM SULFATE, YTTRIUM SULFATE, AND SILICON DIOXIDE

5-1. Introduction

The Na_2SO_4-$Ln_2(SO_4)_3$-SiO_2 solid electrolyte can detect the SO_2 gas at 973 K. However, it is more applicable if the electrolyte can operate at a temperature lower than 973 K. In this chapter, lithium sulfate was mixed with sodium sulfate for the purpose of obtaining a high ionic conductive phase at relatively low temperature(<600^{o}C). Yttrium sulfate and silicon dioxide were also mixed so as to enhance the conductivity and to obtain a heat-endurable electrolyte, respectively. Furthermore, the suppression of the phase transition was attempted by the mixing.

5-2. Experimental

Materials: Sodium sulfate(purity:99.99%), lithium sulfate (purity:99.8 %), and silicon dioxide(purity:99.9 %) were purchased from Wako Pure Chemical Industries Ltd. Yttrium oxide(purity:99.9 %) was bought from Shiga Rare Metal Industries Ltd. Yttrium sulfate was prepared by adding

concentrated sulfuric acid to yttrium oxide. Sodium sulfate(Na_2SO_4), lithium sulfate(Li_2SO_4), yttrium sulfate($Y_2(SO_4)_3$) and silicon dioxide(SiO_2) were dehydrated before weighing. The proper amount of Na_2SO_4, Li_2SO_4, $Y_2(SO_4)_3$, and SiO_2 were mixed thoroughly in an agate mortar. The mixture was melted at 1473 K for 1 h in a platinum crucible in air atmosphere, and then quenched in ice water. The resulting materials were reground and made into pellets under hydrostatic pressure(2.65×10^8 Pa). The pellets were sintered at 1023 K for 2 h in air and quenched in ice water. Platinum powder was sputtered on both center surfaces (5×10^{-3} m) of the electrolyte(1.3×10^{-2} m) with Shimadzu's Ion Coater IC-50.

5-3. Results and Discussion

Phases and thermal properties

X-ray and DTA results for Na_2SO_4-Li_2SO_4-$Y_2(SO_4)_3$-SiO_2 are summarized in Table 13. The doping amounts of Li_2SO_4 and $Y_2(SO_4)_3$ were varied from 5 mol % to 20 mol %, and from 5 mol % to 15 mol %, respectively. All samples except for NO. 7 exhibit a new phase, A, which is similar to Na_2SO_4-I phase. This Na_2SO_4-I phase is a high temperature phase and is appreciably effective for Na^+ ionic conduction. In addition, a small amount of SiO_2 phase coexists. From DTA measurements, the Na_2SO_4-Li_2SO_4-$Y_2(SO_4)_3$-SiO_2 samples, whose doping amount of the Li_2SO_4 and $Y_2(SO_4)_3$ are small, show a endothermic peak at 833 K(NO. 1-3). DTA peaks between 653 K

Table 13. The phases and thermal properties of Na_2SO_4-Li_2SO_4-$Y_2(SO_4)_3$-SiO_2

sample NO.	Na_2SO_4 mol %	Li_2SO_4 mol %	$Y_2(SO_4)_3$ mol %	SiO_2 mol %	phases	DTA peaks K
1	50	5	5	40	A+SiO_2	833(trace)
2	45	10	5	40	A+SiO_2	693(small),833(trace)
3	45	5	10	40	A+SiO_2	833(trace)
4	40	10	10	40	A+SiO_2	733(small)
5	40	5	15	40	A+SiO_2	653(trace)
6	35	10	15	40	A+SiO_2	723(medium)
7	25	20	15	40	B+SiO_2	733(medium),773(medium) 853(medium)

A: Na_2SO_4-I-like phase

B: Unknown phase

and 733 K were obtained for the samples from NO. 4-6 and 2. However, the peaks were considerably small. The peak obtained for NO. 6 was somewhat larger than those for the others. Sample NO. 7 exhibits a different phase(B) from the Na_2SO_4-I phase and shows endothermic peaks at 733, 773, and 853 K.

Electrical conductivity measurements

The temperature dependencies of electrical conductivity for Na_2SO_4-Li_2SO_4-$Y_2(SO_4)_3$-SiO_2 from NO. 1 to 4 are presented in Fig. 33. All samples exhibit almost the same $\log(\sigma T)$-$1/T$ relation. The conductivities at temperatures higher than 571 K are enhanced compared with that of unmixed sodium sulfate. This is attributed to the fact that the cationic conduction occurs more easily when Li_2SO_4 is mixed with Na_2SO_4. However, the σ values of the Na_2SO_4-Li_2SO_4-$Y_2(SO_4)_3$-SiO_2 at lower temperatures(<571 K) are smaller than that of sodium sulfate single phase. The doping of Li_2SO_4 into Na_2SO_4 results in a decrease in the electrical conductivity because the conductivity of the Li_2SO_4 at low temperature is smaller than that of Na_2SO_4. Improvement in the electrical conductivity could not be seen for NO. 1-4. Figure 34 indicates the σT vs. $1/T$ plots for NO. 5 and 6. The $\log(\sigma T)$-$1/T$ curve for NO. 5 is also analogous to those for NO. 1-4. In the case of the sample NO. 6, the electrical conductivities were appreciably enhanced. Furthermore, the $\log(\sigma T)$ vs. $1/T$ plots show almost a straight line relation. A gentler-slope

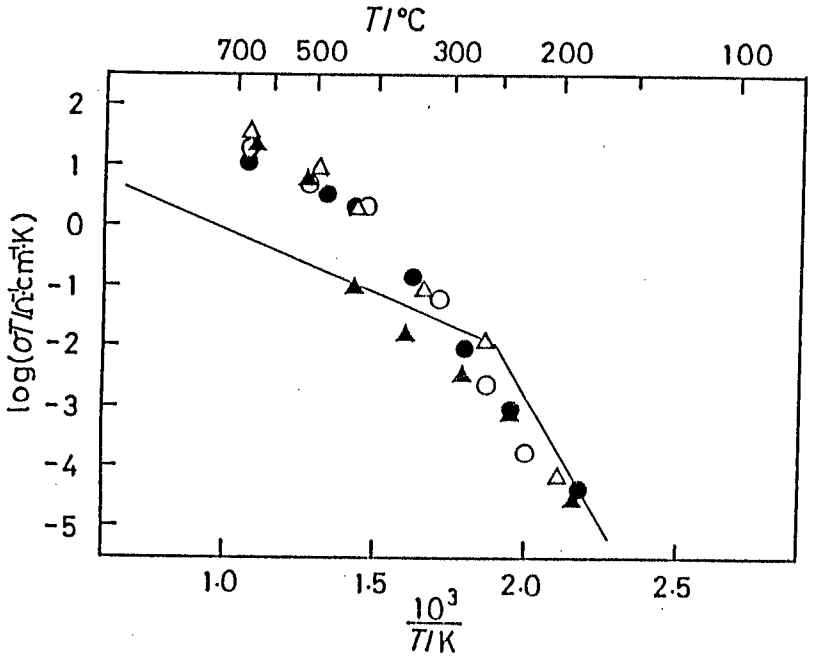

Fig. 33. Temperature dependences of electrical conductivities for Na_2SO_4-Li_2SO_4-$Y_2(SO_4)_3$-SiO_2.

○ Na_2SO_4:Li_2SO_4:$Y_2(SO_4)_3$:SiO_2 = 50: 5: 5:40

△ Na_2SO_4:Li_2SO_4:$Y_2(SO_4)_3$:SiO_2 = 45:10: 5:40

● Na_2SO_4:Li_2SO_4:$Y_2(SO_4)_3$:SiO_2 = 45: 5:10:40

▲ Na_2SO_4:Li_2SO_4:$Y_2(SO_4)_3$:SiO_2 = 40:10:10:40

—— Na_2SO_4

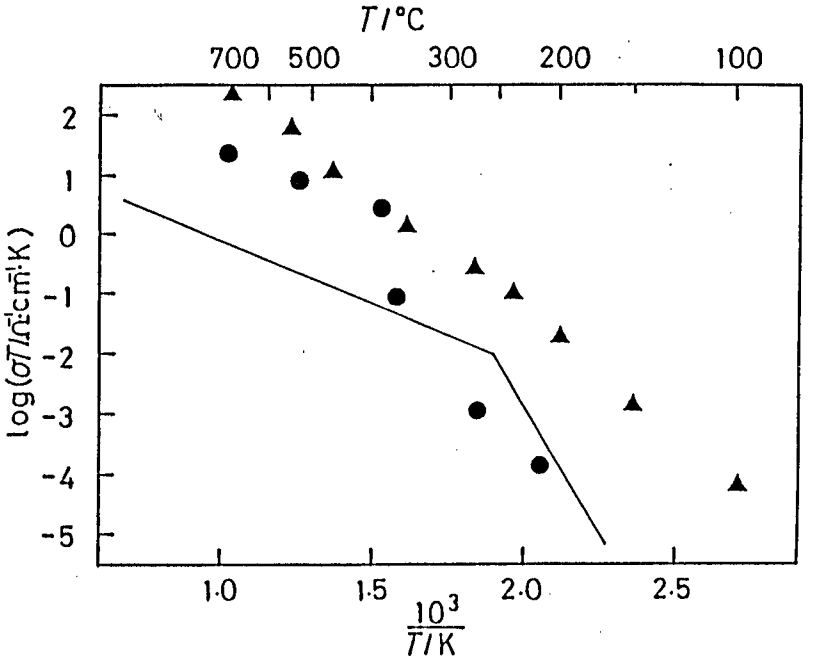

Fig. 34. Temperature dependences of electrical conductivities for Na_2SO_4-Li_2SO_4-$Y_2(SO_4)_3$-SiO_2

● Na_2SO_4:Li_2SO_4:$Y_2(SO_4)_3$:SiO_2 = 40: 5:15:40

▲ Na_2SO_4:Li_2SO_4:$Y_2(SO_4)_3$:SiO_2 = 35:10:15:40

—— Na_2SO_4

relation was obtained for sample NO. 6 compared with that for the others, which means that the σ values are considerably high even at lower temperatures.

From these results, the most appropriate sample for a solid electrolyte as a sulfur dioxide detector is found to be sample NO. 6.

EMF measurements

The electromotive force(EMF) was measured by constructing an SO_2 gas concentration cell with the Na_2SO_4-Li_2SO_4-$Y_2(SO_4)_3$-SiO_2(35:10:15:40) solid electrolyte. The results at 973 K are presented in Fig. 35. In the inlet SO_2 gas concentration from 100 ppm($\log(p_{SO_2})_{in}$ =-4.0) to 1 %($\log(p_{SO_2})_{in}$=-2.0), the measured EMF became higher than that from calculation. However, the difference between the measured and calculated EMF is only about 26 mV and keeps constant in the variation of the sulfur dioxide gas concentration. The longer the electrolyte has been maintained at 973 K, the larger the difference became. The solid electrolyte became ductile even at 973 K because of the mixing of sodium sulfate with lithium sulfate. The interaction between the plastic electrolyte and the platinum net electrode influenced the EMF characteristics and resulted in the higher EMF. The measured EMF at 30 ppm($\log(p_{SO_2})_{in}$= -4.52) was in good agreement with the calculated EMF. However, it is considered that the measured EMF at 30 ppm was about 26 mV smaller than the calculation. The EMF obtained at 973 K was approximately 26 mV larger than the calculated

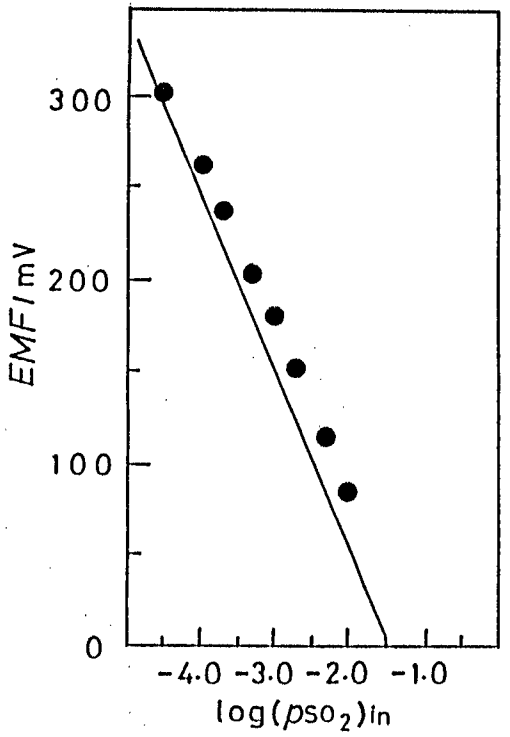

Fig. 35. The variation of the EMF for Na_2SO_4-Li_2SO_4-$Y_2(SO_4)_3$-SiO_2(35:10:15:40) solid electrolyte at 973 K.

——— calculated EMF[3]

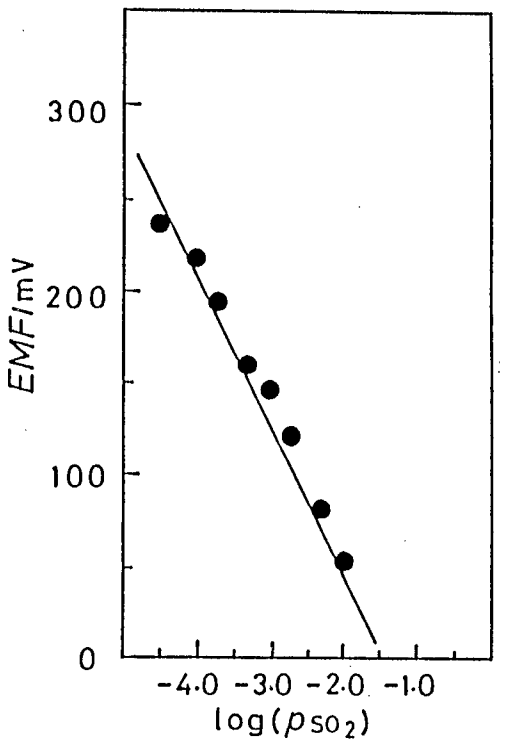

Fig. 36. The variation of the EMF for Na_2SO_4-Li_2SO_4-$Y_2(SO_4)_3$-SiO_2(35:10:15:40) solid electrolyte at 823 K.

——— calculated EMF[3]

EMF. Therefore, the apparently measured EMF at 30 ppm coincided with the calculation. Figure 36 indicates the EMF results at 823 K. The excellent accordance between the measured and calculated EMF was obtained even at 823 K. This temperature is approximately 150 K lower than the temperature where the cation in alkali-metal sulfate is able to predominantly migrate. The EMF measurements at further lower temperature(773 K) are presented in Fig. 37. The measured EMF was fairly in good accordance with the calculation, for the inlet SO_2 gas concentration from

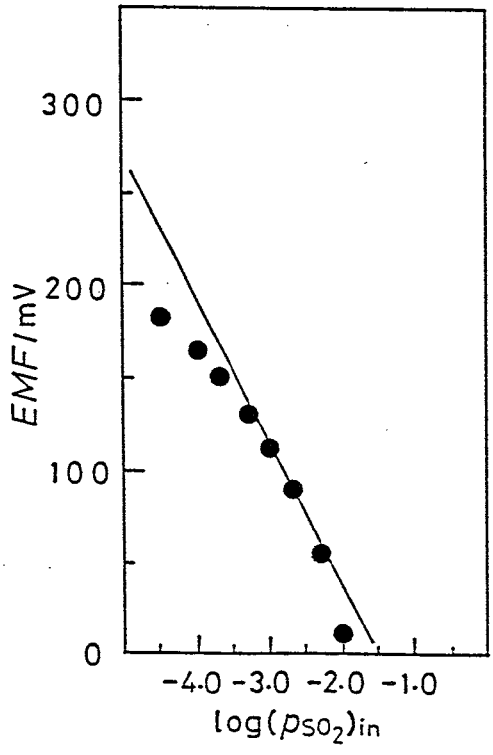

Fig. 37. The variation of the EMF for Na_2SO_4-Li_2SO_4-$Y_2(SO_4)_3$-SiO_2(35:10:15:40) solid electrolyte at 773 K.

——— calculated EMF[3]

500 ppm($\log(p_{SO_2})_{in}$=-3.3) to 0.5 %($\log(p_{SO_2})_{in}$=-2.3). However, the difference between the measured and calculated EMF abruptly increased for inlet SO_2 gas content smaller than 500 ppm. The glass packing is no longer ductile at this temperature(773 K). Many micro-cracks occurred in the glass packing because of the thermal constriction strain difference between the glass packing and the quartz tube. Therefore, the test gas permeated into the reference gas compartment through the cracks. This gas penetration resulted in the EMF decrease. The lower EMF compared with the calculation at 1 % is still in question. Good EMF characteristics were also obtained even at 773 K, which is about 200 K lower than the ordinary operational temperature, for inlet SO_2 gas content between 500 ppm and 0.5 %.

5-4. Summary

Sodium sulfate mixed with lithium sulfate, yttrium sulfate, and silicon dioxide was prepared and its phases, thermal, and electrical properties were investigated. The Na_2SO_4-Li_2SO_4-$Y_2(SO_4)_3$-SiO_2 samples exhibit similar phase to Na_2SO_4-I phase, which is appreciably effective for Na^+ ionic conduction. Phase transformation was considerably suppressed by these mixing. The electromotive force (EMF) was measured with the Na_2SO_4-Li_2SO_4-$Y_2(SO_4)_3$-SiO_2 solid electrolyte by constructing an SO_2 gas concentration cell. The measured EMF at 823 K and 773 K were in fairly good accordance with the calculated EMF, in the inlet SO_2 gas

concentration between 30 ppm and 1 %, and 500 ppm and 0.5 %, respectively.

Chapter 6

THE EMF MEASUREMENTS WITH MSO_4-MO_x(M=Ni, Mn, Mg, Co) SOLID REFERENCE ELECTRODE METHOD

6-1. Introduction

In the laboratory, the SO_2 gas concentration cell method using the solid electrolyte is considered to be a good technique for detecting the SO_2 gas. However, in a practical utilization, the method is not suitable, particularly because the apparatus is expensive and complicated. The solid reference electrode method was examined in order to approach a more practical application.

6-2. Experimental

The apparatus for the solid reference electrode method is depicted in Fig. 38. The solid electrolyte was directly kept in contact with the solid reference electrode by fixing the reference platinum electrode between them. The sample is covered with a bonding agent(SUMICERAM from Sumitomo Chemical Industries Ltd). As a solid reference electrode, the equimolar mixture of metal sulfate and metal oxide was applied. As metal sulfates, $NiSO_4$, $MnSO_4$, $MgSO_4$, and $CoSO_4$ were selected because the melting temperature of them is higher

than the operating temperature.

6-3. Results and Discussion

Na_2SO_4-$Y_2(SO_4)_3$-SiO_2 system

The results of the EMF measurements with the $NiSO_4$-NiO solid reference electrode at 973 K are shown in Fig. 39 together with the results of Na_2SO_4 as a comparison. The EMF characteristics for Na_2SO_4 decreased significantly in the inlet SO_2 gas concentration less than 0.1 %($\log(P_{SO_2})_{in}$=-3.0) because of the gas permeation through cracks occurred in the electrolyte. In the case of the Na_2SO_4-$Y_2(SO_4)_3$-SiO_2 electrolyte, the measured EMF was in good accordance with the calculated EMF, in the inlet SO_2 gas concentration from 30 ppm($\log(P_{SO_2})_{in}$=-4.52) to 1 %. No chemical reaction between the electrolyte and the $NiSO_4$-NiO reference electrode was observed. The EMF results with the $MgSO_4$-MgO_2 solid reference electrode at 973 K are shown in Fig. 40. The values obtained were approximately 280 mV higher than the calculated EMF. The $MgSO_4$-MgO reference electrode seemed to react with the Na_2SO_4-$Y_2(SO_4)_3$-SiO_2 solid electrolyte during measurement. This chemical reaction might considerably enhance the EMF value. The variation of the EMF with the $MnSO_4$-Mn_2O_3 solid reference electrode at 973 K is also presented in Fig. 41. In all measurements, the measured EMF was about 80 mV larger than the calculated value. The $MnSO_4$-Mn_2O_3 electrode, however, did not react with the electrolyte. The difference between the measured and the calculated EMF can be mainly

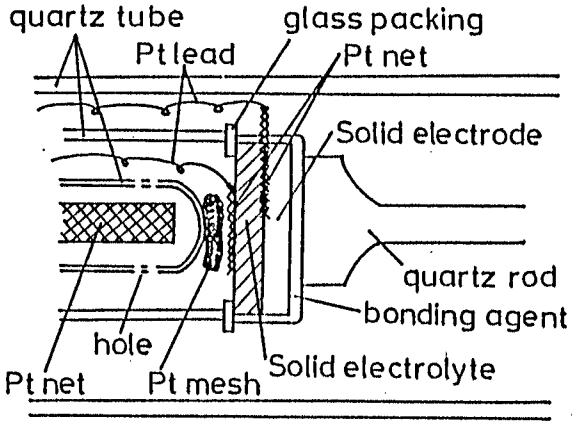

Fig. 38. The apparatus for the EMF measurements. (A solid reference electrode method)

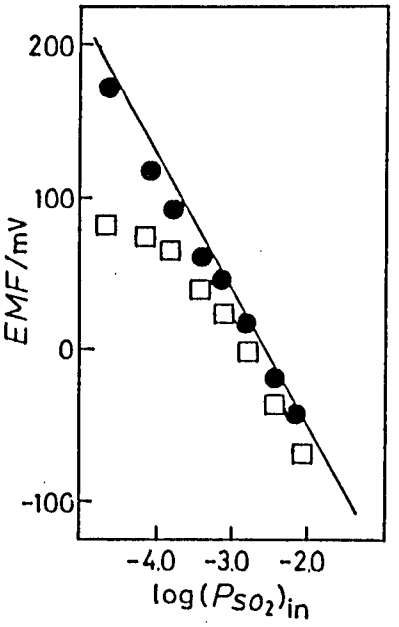

Fig. 39. The variation of the EMF for Na_2SO_4 and Na_2SO_4-$Y_2(SO_4)_3$-SiO_2(48.1:11.8:40.1) solid reference electrode method ($NiSO_4$-NiO)

● Na_2SO_4-$Y_2(SO_4)_3$-SiO_2

□ Na_2SO_4

—— calculated EMF[9]

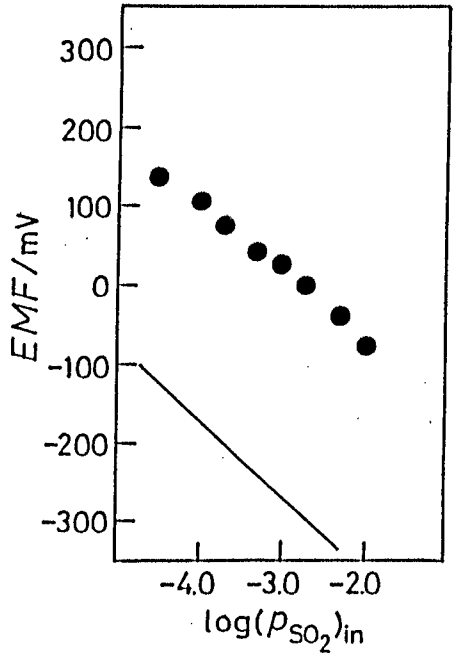

Fig. 40. The variation of the EMF for Na_2SO_4-$Y_2(SO_4)_3$-SiO_2(48.1:11.8:40.1) solid electrolyte with the solid reference electrode method($MgSO_4$-MgO)

———— calculated EMF[9]

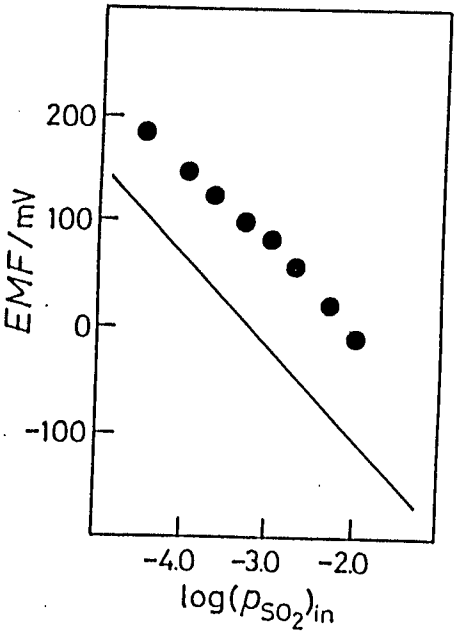

Fig. 41. The variation of the EMF for Na_2SO_4-$Y_2(SO_4)_3$-SiO_2(48.1:11.8:40.1) solid electrolyte with the solid reference electrode method($MnSO_4$-Mn_2O_3)

———— calculated EMF[9]

ascribed to the fact that manganese oxides of different oxidation states may have been produced. The EMF results with $CoSO_4$-CoO solid reference electrode are presented in Fig. 42. The measured EMF exceeded the calculated EMF about 80 mV. Rapid reaction between the solid electrolyte and $CoSO_4$-CoO electrode was not recognized. However, the color of the elctrode was changed from deep purple to black after the measurement. This phenomenon means that the decomposition of the $CoSO_4$ has been considerably proceeded. Because of this decomposition, the SO_3 partial pressure enhanced and

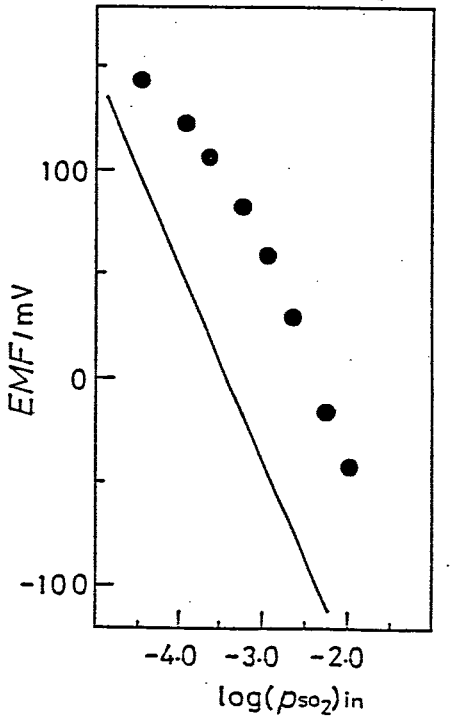

Fig. 42. The variation of the EMF for Na_2SO_4-$Y_2(SO_4)_3$-SiO_2(48.1:11.8:40.1) solid electrolyte with the solid reference electrode method ($CoSO_4$-CoO)

———— calculated EMF[9,49]

resulted in the increase in the EMF value. In order to suppress this decomposition, an alumina plate was devised to separate the electrolyte and the electrode.

The apparatus for the EMF measurements with an alumina plate between the electrolyte and the electrode is shown in Fig. 43.

The EMF results with $CoSO_4$-CoO solid reference electrode is presented in Fig. 44. The measured EMF was in good agreement with the calculated EMF, in the SO_2 gas region from 30 ppm to 1 %. This means that the decomposition reaction has been appreciably supressed. The EMF measurement with $MgSO_4$-MgO solid reference electrode is exhibited in Fig. 45. The EMF was appreciably enhanced compared with the calculated value. The chemical reaction between the electrolyte and the $MgSO_4$-MgO solid electrode could not be supressed even if an alumina plate was inserted between them.

Na_2SO_4-$Ln_2(SO_4)_3$-Al_2O_3 systems(Ln=La and Y)

Figure 46 indicates the EMF results for the Na_2SO_4-$La_2(SO_4)_3$-Al_2O_3 with solid reference electrode method($NiSO_4$-NiO) at 973 K. The EMF coincides with the calculation, in the inlet SO_2 gas concentration between 100 ppm and 1 %. The measured EMF was about 30 mV lower than the calculated EMF at 30 ppm. This result refers to the gas penetration through the microcracks in the electrolyte. The EMF results for Na_2SO_4-$Y_2(SO_4)_3$-Al_2O_3 with $NiSO_4$-NiO solid reference electrode is presented in Fig. 47. The measured EMF is consistent with the calculated EMF from 500 ppm to 1 %. However, the discrepancy

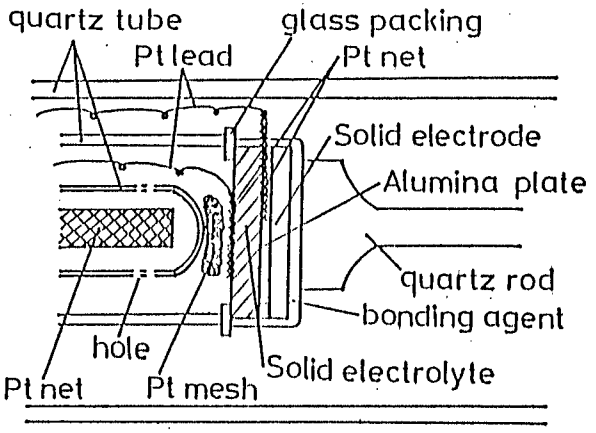

Fig. 43. The apparatus for the EMF measurements (A metal sulfate-metal oxide reference electrode method)

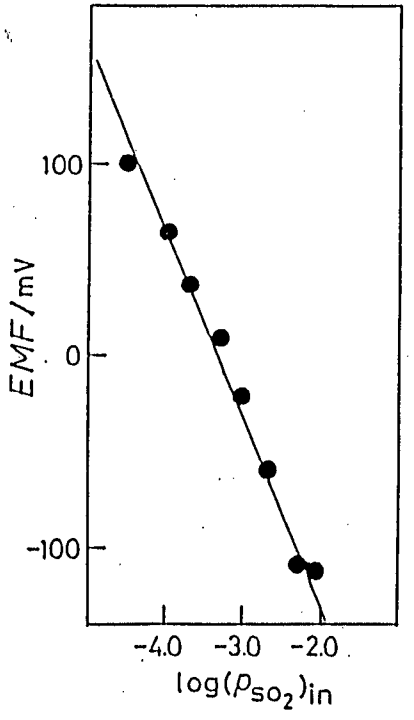

Fig. 44. The variation of the EMF for Na_2SO_4-$Y_2(SO_4)_3$-SiO_2 (48.1:11.8:40.1) solid electrolyte with the solid reference electrode method ($CoSO_4$-CoO)

● Al_2O_3 plate between electrolyte and electrode

—— calculated EMF [9,49]

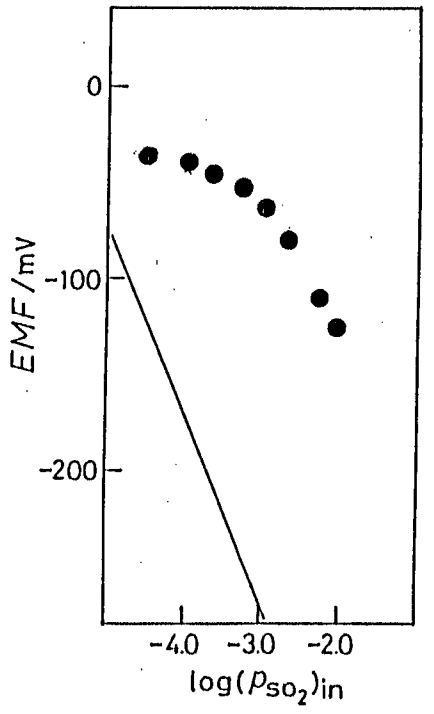

Fig. 45. The variation of the EMF for Na_2SO_4-$Y_2(SO_4)_3$-SiO_2(48.1:11.8:40.1) solid electrolyte with the solid reference electrode method($MgSO_4$-MgO)

● Al_2O_3 plate between electrolyte and electrode

—— calculated EMF[9]

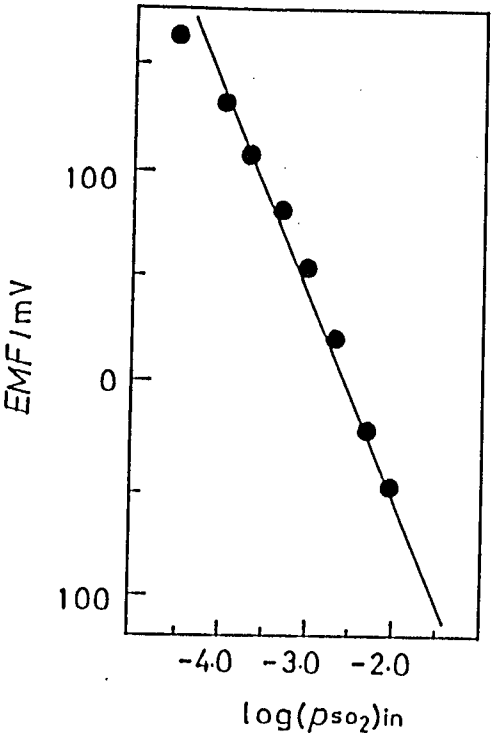

Fig. 46. The variation of the EMF for Na_2SO_4-$La_2(SO_4)_3$-Al_2O_3(44.8:15.3:39.9) solid electrolyte with the solid reference electrode method($NiSO_4$-NiO)

———— calculated EMF[9]

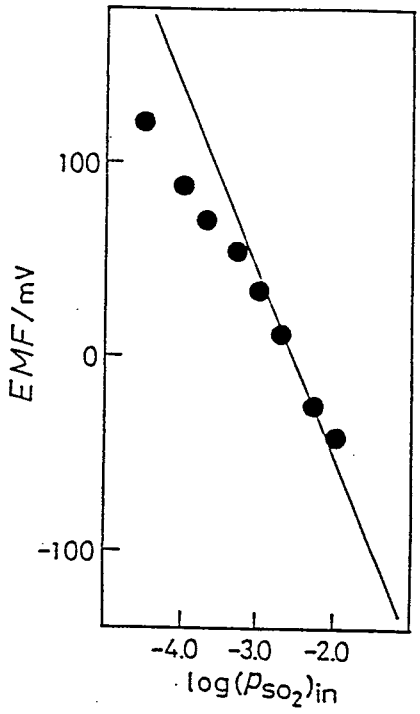

Fig. 47. The variation of the EMF for Na_2SO_4-$Y_2(SO_4)_3$-Al_2O_3(48:12:40) solid electrolyte with the solid reference electrode method($NiSO_4$-NiO) at 973 K.

———— calculated EMF[9]

between the measured and calculated EMF becomes largher in the SO_2 gas concentration region less than 500 ppm. Because of no phase transformation, the decrease in the lower SO_2 gas content for the Na_2SO_4-$Y_2(SO_4)_3$-Al_2O_3 electrolyte, is ascribed to the gas penetration through the glass packing. The results with $CoSO_4$-CoO and $MgSO_4$-MgO are also shown in Fig. 48 and 49, respectively. Both electrode methods exhibit higher EMF compared with calculation because of the reaction between the electrolyte and the electrode in spite of the insertion of the alumina plate.

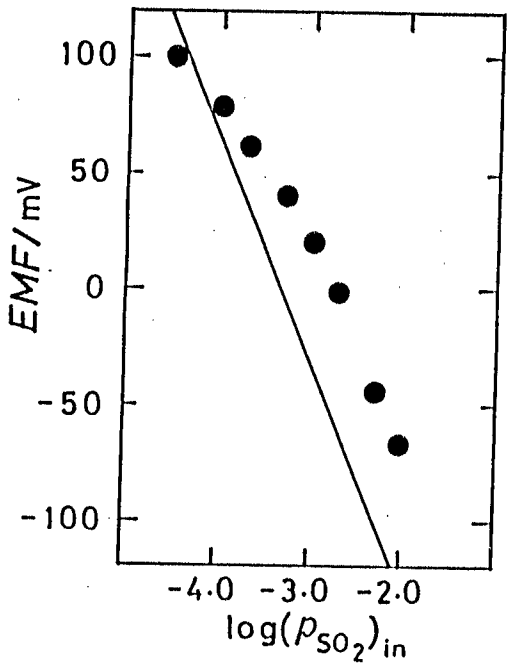

Fig. 48. The variation of the EMF for Na_2SO_4-$Y_2(SO_4)_3$-Al_2O_3(48:12:40) solid electrolyte with the solid reference electrolyte method($CoSO_4$-CoO) at 973 K.

——— calculated EMF[9,49]

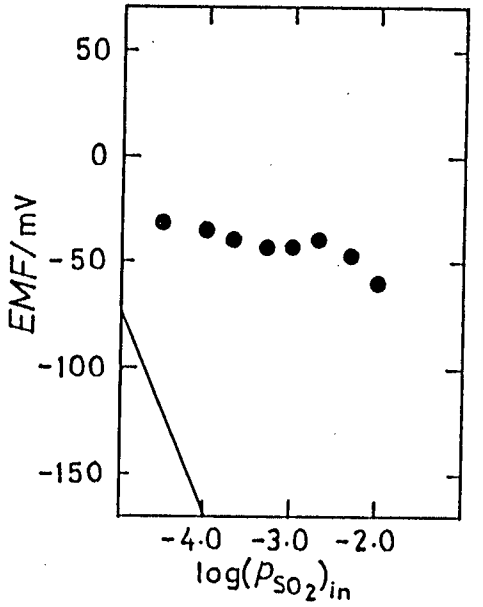

Fig. 49. The variation of the EMF for Na_2SO_4-$Y_2(SO_4)_3$-Al_2O_3(48:12:40) solid electrolyte with the solid reference electrode method($MgSO_4$-MgO) at 973 K.

——— calculated EMF[9]

Na_2SO_4-Li_2SO_4-$Y_2(SO_4)_3$-SiO_2 system

Figure 50 shows the EMF results with $NiSO_4$-NiO solid reference electrode. The EMF slightly deviates to the lower compared with the calculation in the SO_2 gas content smaller than 200 ppm. The measured EMF is in good accordance with the calculated EMF in the SO_2 gas higher than 200 ppm. The EMF results with $CoSO_4$-CoO electrode is presented in Fig. 51.

Almost the same EMF as calculation was obtained in the region 30 ppm to 0.5 %

6-4. Summary

The electrolyte with $NiSO_4$-NiO reference electrode also shows superior EMF results for the SO_2 gas content from 30 ppm to 1 %. The method has the advantage of making the cell more compact, lighter, and less expensive compared with the SO_2 gas concentration cell method. The solid reference electrode method with $CoSO_4$-CoO can be utilized longer because the decomposition pressure of $CoSO_4$ is smaller than that of $NiSO_4$. Furthermore, sodium sulfate mixed with rare earth sulfate and aluminum oxide, and sodium sulfate mixed with lithium sulfate and yttrium sulfate, and silicon dioxide, contain Na_2SO_4-I phase and exhibit higher electrical conductivity compared with sodium sulfate. The Na_2SO_4-Li_2SO_4-$Y_2(SO_4)_3$-SiO_2 electrolytes show excellent EMF characteristics with the $NiSO_4$-NiO solid reference electrode in the SO_2 gas range from 100 ppm to 1 %, and with the $CoSO_4$-CoO electrode from 30 ppm

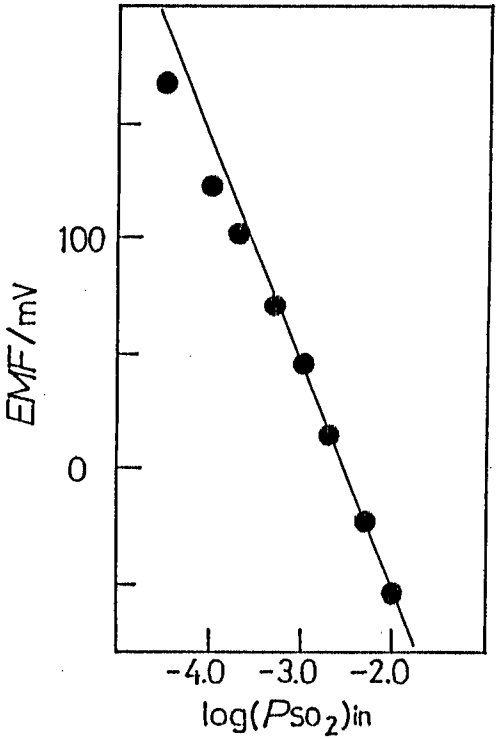

Fig. 50. The variation of the EMF for Na_2SO_4-Li_2SO_4-$Y_2(SO_4)_3$-SiO_2(35:10:15:40) solid electrolyte with the solid reference electrode method($NiSO_4$-NiO) at 973 K.

———— calculated EMF[9]

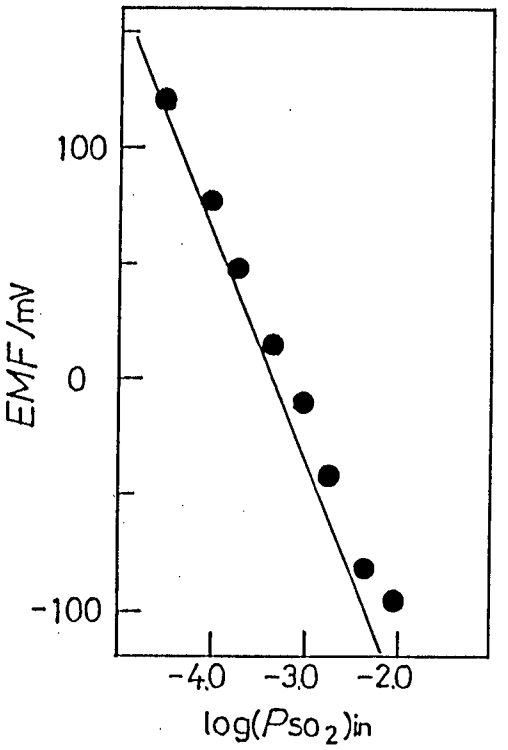

Fig. 51. The variation of the EMF for Na_2SO_4-Li_2SO_4-$Y_2(SO_4)_3$-SiO_2(35:10:15:40) solid electrolyte with the solid reference electrode method($CoSO_4$-CoO) at 973 K.

———— calculated EMF[9,49]

to 0.5 %, respectively.

Chapter 7

CONCLUDING REMARKS

In this thesis, sodium sulfate-based solid electrolytes have been prepared and their electrical and thermal properties were investigated. Furthermore, the EMF measurements were conducted at first with a sulfur dioxide gas concentration cell method, and then a solid reference electrode method for the purpose of applying in practical applications. Main results of this work are as follows.

1. Sodium sulfate doped with $NaVO_3$ and $Ln_2(SO_4)_3$(Ln=Pr and Y) has suitable properties for the solid electrolyte because the solid solution shows considerably high electrical conductivity. The sulfate can be utilized as the solid electrolyte for an SO_2 gas sensor even at 673 K which is approximately 300 K lower than pure sodium sulfate can be used. The doping of sodium vanadate as well as rare earth sulfates makes considerable progress in the improvement of the electrolyte.

2. Sodium sulfate mixed with $Ln_2(SO_4)_3$(Ln=Y and Gd) and SiO_2 maintains relatively high electrical conductivities. When Na_2SO_4-$Ln_2(SO_4)_3$-SiO_2(Ln=Y and Gd) are applied as solid electrolytes for a sulfur dioxide gas sensor, they can detect the SO_2 gas in the inlet SO_2 gas concentration range from 0.1 % to 23 %, and 0.32 % to 10 %, respectively. In addition,

the platinum sputtering on both center surfaces of the electrolyte contributes to the enhancement of the EMF results for the SO_2 gas content between 30 ppm and 1000 ppm.

3. Sodium sulfate mixed with rare earth sulfate and aluninum oxide contains Na_2SO_4-I-similar phase and higher conductivity compared with unmixed sodium sulfate at 973 K. The EMF characteristics for the Na_2SO_4-$Ln_2(SO_4)_3$-Al_2O_3 solid electrolyte were fairly in good accordance with the calculated EMF , in the inlet SO_2 gas content between 100 ppm and 1 %.

4. Sodium sulfate mixed with lithium sulfate, yttrium sulfate, and silicon dioxide exhibits a similar phase to Na_2SO_4-I, which is appreciably effective in Na^+ cationic conduction. Furthermore, the electrical conductivity of the Na_2SO_4-Li_2SO_4-$Y_2(SO_4)_3$-SiO_2(35:10:15:40) solid electrolyte is about 320 times higher than unmixed sodium sulfate at 973 K. In the inlet SO_2 gas concentration from 30 ppm to 1 %, the measured EMF coincides with the calculated EMF even at 823 K, which is approximately 150 K lower than the operational temperature for unmixed alkali-metal sulfates. In addition, the Na_2SO_4-Li_2SO_4-$Y_2(SO_4)_3$-SiO_2 electrolyte can detect the SO_2 gas between 500 ppm and 0.5 %, at a temperature of 773 K.

5. The solid reference electrode method of the Na_2SO_4-$Y_2(SO_4)_3$-SiO_2 solid electrolyte with $NiSO_4$-NiO solid reference elec-

trode shows excellent EMF results for the SO_2 gas content between 30 ppm and 1 %. The method is excellent to make the cell more compact, lighter, and less expensive in comparison to an SO_2 gas concentration cell method.

6. The solid reference electrode method with $CoSO_4$-CoO also exhibits as good EMF characteristics as with $NiSO_4$-NiO by inserting an alumina plate between the electrolyte and the electrode. The $CoSO_4$-CoO electrode has the advantage in being utilized longer because the decomposition pressure of $CoSO_4$ is smaller than that of $NiSO_4$. The method with metal sulfate-metal oxide electrode has a potential in a practical application.

7. Sodium sulfate mixed with rare earth sulfate and aluminum oxide, and sodium sulfate mixed with lithium sulfate, yttrium sulfate, and silicon dioxide, maintain Na_2SO_4-I phase and show higher electrical conductivity in comparison with sodium sulfate. Especially, the Na_2SO_4-Li_2SO_4-$Y_2(SO_4)_3$-SiO_2 electrolyte exhibits superior EMF characteristics with the $NiSO_4$-NiO solid reference electrode for the SO_2 gas region between 100 ppm and 1 %, and with the $CoSO_4$-CoO electrode between 30 ppm and 0.5 %, respectively.

ACKNOWLEDGEMENT

The author is greatly indebted to Professor Jiro Shiokawa at the Department of Applied Chemisrty, Faculty of Engineering, Osaka University for his continuous guidance and encouragement throughout this work.

The author is also indebted to Professor Toshio Tanaka and Professor Hiroshi Yoneyama for their kind suggestions in the course of this thesis.

The author would like to express his sincere thanks to Associate Professor Gin-ya Adachi for his significant direction during the course of the study, and for his kind discussion in the preparation of the manuscript.

The author would like to acknowledge Dr. Yoshiyuki Hirashima, Dr. Tsuyoshi Arakawa, and Dr. Tsutomu Shin-ike for their significant discussion.

Thanks are given to the author's co-workers, Mr. Yasuo Yamaguchi, Mr. H. Yoshioka, Mr. Kenji Kawai, and Mr. Shigeru Kuwabara for their assistance, and Dr. Mineo Sato, Dr. Tetsuo Sakai, Dr. Ken-ichi Machida, Dr. Kenji Ishikawa, Mrs. Ichiko kawamoto, Mrs. Maki Kitora, Mr. Hiroki Sakaguchi, Mr. Shigeharu Matsubayashi, Mr. Hai-feng Wang, and all the other members of Shiokawa group for their help and valuable suggestions.

Finally, the author wishes to express his gratitude to his parents and wife from the bottom of his heart for their encouragement and understanding on this work.

References

1. Y. Saito and T. Maruyama, Nippon Kinzoku Gakkai Shi, 23, 30 (1984).
2. Y. Saito, T. Maruyama, and S. Sasaki, Hyomen Kagaku, 5, 76 (1984).
3. K. T. Jacob and D. B. Rao, J. Electrochem. Soc., 126, 1842 (1979).
4. W. L. Worrell, Proc. the International Meeting on Chemical Sensors, Fukuoka, 1983, p. 332.
5. W. L. Worrell and Q. G. Liu, J. Electroanal. Chem., 168, 355 (1984).
6. M. Gauthier and A. Chamberland, J. Electrochem. Soc., 124, 1579 (1977).
7. M. Gauthier, A. Chamberland, A. Bélanger, and M. Poirier, J. Electrochem. Soc., 124, 1584 (1977).
8. M. Gauthier, R. Bellemare, and A. Bélanger, J. Electrochem. Soc., 128, 371 (1981).
9. M. Gauthier and C. W. Bale, Metall. Trans. B. 14B, 117 (1983).
10. A. Bélanger, M. Gauthier, and D. Fauteux, J Electrochem. Soc., 131, 579 (1984).
11. Y. Saito, T. Maruyama, Y. Matsumoto, K. Kobayashi, and Y. Yano, Solid State Ionics, 14, 273 (1984).
12. M. Itoh, E. Sugimoto, and Z. Kozuka, Trans. Jpn. Inst. Met., 25, 504, (1984).
13. E. Sugimoto, Y. Tanizawa, and Z. Kozuka, Jpn. Kokai Tokkyo Koho JP 58/214851.

14. Z. Kozuka, M. Itoh, and E. Sugimoto, Jpn. Kokai Tokkyo Koho JP 60/3547.

15. Z. Kozuka, M. Itoh, E. Sugimoto, and S. Iishima, JP 60/58549.

16. Y. Saito, T. Maruyama, Y. Matsumoto, and Y. Yano, Proc. the International Meeting on Chemical Sensors, Fukuoka, 1983, p. 326.

17. Y. Saito, T. Maruyama, and S. Sasaki, Report of the Research Laboratory of Engineering Materials, Tokyo Institute of Technology, 9, 17 (1984).

18. H. Y-P. Hong, Mater. Res. Bull., 11, 173 (1976).

19. J. B. Goodenough, H. Y-P. Hong, and J. A. Kafalas, Mater. Res. Bull., 11, 203 (1976).

20. U. v. Alpen, M. F. Bell, and W. Wichelhaus, Mater. Res. Bull., 14, 1317 (1979).

21. J. P. Boilot, J. P. Salanié, G. Desplanches, and D. Le Potier, Mater. Res. Bull., 14, 1469 (1979).

22. R. S. Corden, G. R. Miller, B. J. McEntire, E. D. Beck, and J. R. Rasmussen, Solid State Ionics, 3/4, 243 (1981).

23. T. Takahashi, K. Kuwabara, and M. Shibata, Solid State Ionics, 1, 163 (1980).

24. W. Bogusz, F. Krok, and W. Jakubowski, Solid State Ionics, 2, 171 (1981).

25. U. v. Alpen, M. F. Bell, and H. H. Höfer, Solid State Ionics, 3/4, 215 (1981).

26. J. P. Coughlin, J. Am. Chem. Soc., 77, 868 (1955).

27. Y. A. Badr, F. El-Kabbany, and M. Tosson, Phys. Status Solidi A, 53, K51 (1979).

28. F. El-Kabbany, Y. Badr, and M. Tosson, Phys. Status Solidi A, 63, 699 (1981).

28. Q. R. Goyal, V. V. Deshpande, and M. D. Karkhanavala, Indian J. Chem., 9, 1006 (1971).

30. J. E. D. Davies and W. F. Sandford, J. Chem. Soc., Dalton Trans., (1975) 1912.

31. B. N. Mehrotra, Th. Hahn, H. Arnold and W. Eysel, Acta Crystallogr., Sect. A, 31, S79 (1975).

32. V. Amirthalingam, M. D. Karkhanavala, and U. R. K. Rao, Acta Crystallogr., Sect. A, 33, 522 (1977).

33. C. A. Cody, L. Dicarlo, and R. K. Darlington, J. Inorg. Nucl. Chem., 43, 398 (1981).

34. F. C. Kracek, J. Phys. Chem., 33, 1281 (1929).

35. F. C. Kracek and R. E. Gibson, J. Phys. Chem., 33, 1304 (1929).

36. F. C. Kracek and R. E. Gibson, J. Phys. Chem., 34, 188 (1930).

37. F. C. Kracek and C. J. Ksanda, J. Phys. Chem., 34, 1741 (1930).

38. G. E. Brodale and W. F. Giauque, J. Phys. Chem., 76, 737 (1972).

39. E. L. Kreidl and Ivan Simon, Nature, 181, 1529 (1958).

40. Y. Saito, K. Kobayashi, and T. Maruyama, Thermochim. Acta, 53, 289 (1982).

41. K. Kobayashi and Y. Saito, Thermochim. Acta, 53, 299 (1982).

42. Y. Saito, K. Kobayashi, and T. Maruyama, Solid State Ionics, 3/4, 393 (1981).

43. H. H. Höfer, W. Eysel, and U. v. Alpen, J. Solid State Chem., 36, 365 (1981).

44. H. H. Höfer, W. Eysel, and U. v. Alpen, Mater. Res. Bull., 13, 265 (1978).

45. R. M. Murray and E. A. Secco, Can. J. Chem., 56, 2616 (1978).

46. K. L. Keester, W. Eysel, and Th. Hahn, Acta Crystallogr., Sect. A, 31, S79 (1975).

47. H. H. Höfer, U. v. Alpen, and W. Eysel, Acta Crystallogr., Sect. A, 34, S358 (1978).

48. J. E. Bauerle, J. Phys. Chem. Solids, 30, 2657 (1969).

49. H. H. Kellogg, Trans. Metal. Soc. AIME, 230, 1622 (1964).